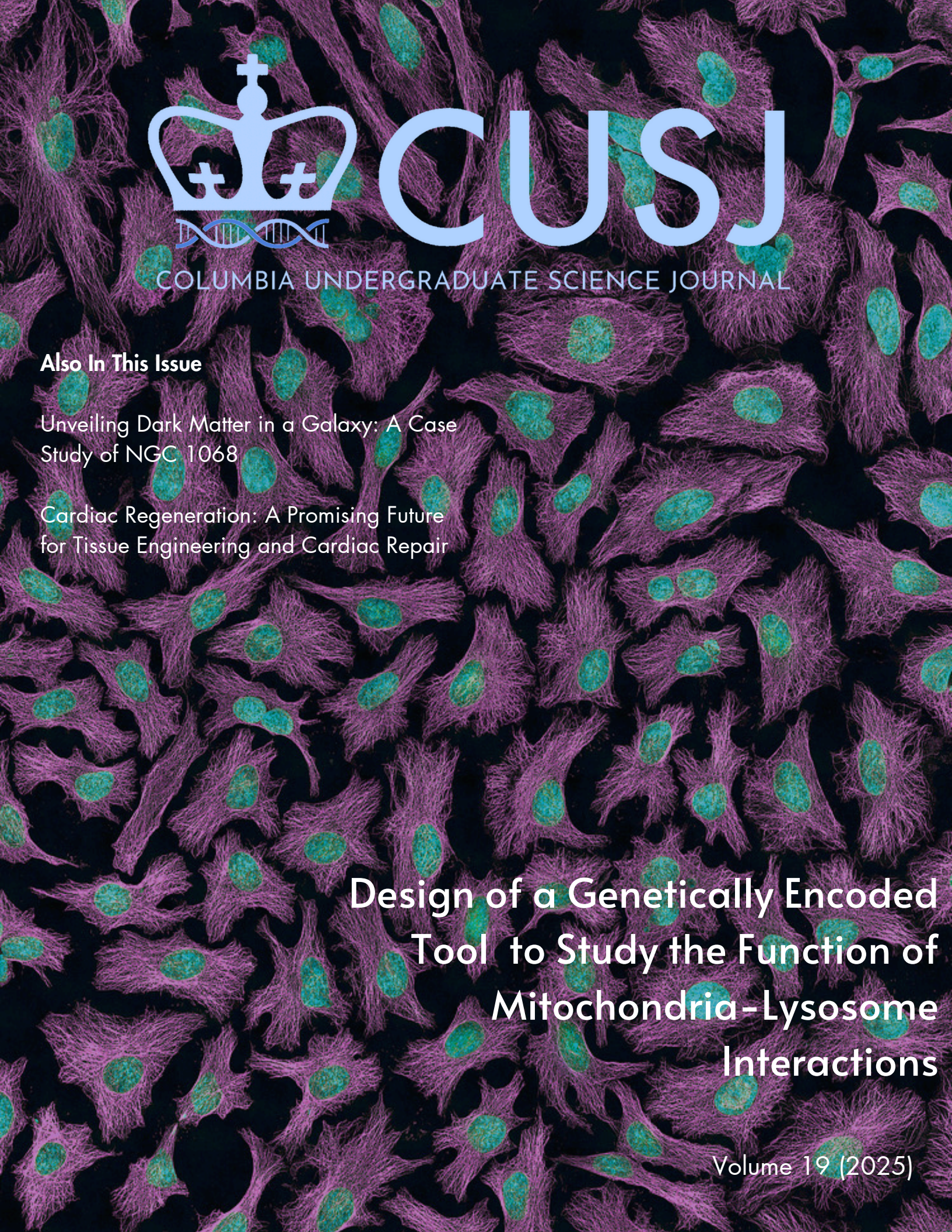

CUSJ

COLUMBIA UNDERGRADUATE SCIENCE JOURNAL

Also In This Issue

Unveiling Dark Matter in a Galaxy: A Case Study of NGC 1068

Cardiac Regeneration: A Promising Future for Tissue Engineering and Cardiac Repair

Design of a Genetically Encoded Tool to Study the Function of Mitochondria-Lysosome Interactions

Volume 19 (2025)

About the Journal

Aims and Scope

The Columbia Undergraduate Science Journal (CUSJ) was founded in 2006 by students who were passionate about showcasing undergraduate excellence in scientific research. Since then, CUSJ has remained Columbia's premier publication for original scientific research and scholarly reviews and is managed by an editorial board of undergraduates with a vast scope of interests across all disciplines. The editorial board also manages the Columbia Junior Science Journal (CJSJ), a publication designed to introduce high school students to research, and Columbia Scientist, a publication aimed at increasing scientific engagement and thought at all academic levels. In addition to our publications, the CUSJ team is dedicated to fostering the scientific community, both within Columbia and in the surrounding Morningside Heights and Harlem communities. To this end, the board frequently plans outreach and networking events relevant to young and early career scientists, including an annual Research Symposium poster session each spring.

Copyrights and Permissions

Contact

Email cusj@columbia.edu with any inquiries. Visit cusj.columbia.edu for more information about the journal.

COLUMBIA UNDERGRADUATE SCIENCE JOURNAL

Letter from the Editor-in-Chief

Dear Readers,

As the academic year comes to an end, we are eager to share the Spring 2025 Columbia Undergraduate Science Journal. This year, our team has continued to work on increasing efforts to highlight undergraduate research and scientific thought. Since 2006, CUSJ has created an environment to promote scientific journalism among undergraduates and this edition emphasizes those values.

This edition features a broad range of topics from astrophysics to tissue engineering. We thank each author for sharing their curiosity and encourage all our readers to partake in pushing for scientific discovery. Our community strongly supports the role of science in society and recognizes the role of mentorship and support in providing an accessible way for undergraduate researchers to present their work.

With that, I would like to express my gratitude to our editorial team for their tireless dedication to our journal. Publishing this journal is a testament to the hard work of our editors and I am especially grateful for everyone's insightful feedback and commitment throughout the year. Additionally, I want to extend my appreciation to all members of CUSJ for their teamwork and support for our editors in publishing the highest quality articles.

It would not be possible to undertake the goal of encouraging undergraduate scientific research alone which is why I thank and acknowledge the CUSJ executive board for their leadership and guidance. Every committee works hard to uphold the standards of our journal while sharing our vision and our leaders have put in a tremendous amount of work to maintain our community. Furthermore, I sincerely appreciate the Faculty Advisory Board and Columbia Libraries for their assistance which has been essential in allowing us to sustain our high standards of academic excellence.

It has been my honor to serve as Editor-in-Chief for the Spring 2025 edition of CUSJ. As I step down from my position, I hold pride in knowing that this journal will exceed expectations with its rigorous editing. Thank you for supporting CUSJ and I hope you enjoy this edition as much as we enjoyed creating it.

Sincerely,
Amanda Prashad
Editor-in-Chief, Columbia Undergraduate Science Journal

COLUMBIA UNDERGRADUATE SCIENCE JOURNAL

Letter from the President

Dear Readers,

I proudly present to you the Spring edition of CUSJ — one of three journals encompassed by our open-access organization. As our original and signature journal, CUSJ remains a crucial space to highlight cutting-edge research driven by undergraduate researchers. Founded 19 years ago, CUSJ continues its mission of showing excellence in scientific research with the most rigorous standards. Each and every season, we begin our nationwide search for the most talented young scientists and the discoveries they have made. This season's edition exemplifies our founding purpose in the knowledge they bring forth.

I commend our authors for their dedicated pursuit of truth in the form of scientific research. From research exploring the cosmos to new developments in tissue engineering, our selected works reflect a diverse range of innovations dedicated to enhancing our understanding of the world.

Our work does not exist in a vacuum — instead, it exists in the context of what we hope to achieve from our research as scientists. Ultimately, we hope to impact humankind. We strive to understand so that we may apply our knowledge for the benefit of humanity. This edition is a profound reflection of that sentiment.

As we celebrate the release of the Spring edition of CUSJ, we complete our transition to the next executive board. As I write my final letter to our readers, I reflect on the great privilege of serving as CUSJ's president. Four years ago, I was a young reader of CUSJ, hoping one day to be at Columbia and a part of this great organization. Today, I complete my term as President and hand down the legacy and mission of CUSJ to our brilliant incoming executive board.

Lastly, I thank Editor-in-Chief Amanda Prashad for her incredible work in her years at CUSJ. At CUSJ, we pride ourselves on being more than an organization; we are a community of leaders and editors who lead by example and integrity. Amanda exemplifies these qualities and we, both, look forward to seeing the bright future of our authors and organization.

With gratitude,
Kayla Pham
CUSJ President

COLUMBIA UNDERGRADUATE SCIENCE JOURNAL

Masthead

Editors

Faculty Advisory Board

CUSJ
COLUMBIA UNDERGRADUATE SCIENCE JOURNAL

Table of Contents

Administrative

Selected Works

CUSJ
COLUMBIA UNDERGRADUATE SCIENCE JOURNAL

Design of a Genetically Encoded Tool to Study the Function of Mitochondria–Lysosome Interactions

Yuliia Kohut[1], Robert Coukos[1], Dimitri Krainc[1]

[1]Department of Neurology, Northwestern University Fienberg School of Medicine, Chicago, IL, USA

KEYWORDS: Biosynthetic tools, membrane contact sites, mitochondria-lysosome contacts, ABI-PYL domain, immunofluorescence, confocal microscopy, neurodegeneration

ABSTRACT: Membrane contact sites are regions of close proximity between organelles that mediate crucial organelle functions. However, the list of effective biological tools to study membrane contact sites function still needs expansion. Mitochondria and lysosomes are organelles whose dysfunctions are closely associated with Parkinson's disease pathology, and some Parkinson's disease-associated genes have been shown to play a role in mitochondria-lysosome contact regulation. A novel biosynthetic system for reversible induction of interactions between mitochondria and lysosomes is presented, leveraging abscisic-acid-mediated heterodimerization of ABI and PYL protein domains from *Arabidopsis thaliana*. Combinations of genetically encoded protein heterodimer constructs each containing the ABI or PYL domain, a fluorescent protein tag (EGFP, mCherry, iRFP, or BFP), and a transmembrane sequence targeting the lysosomal membrane or outer mitochondrial membrane were engineered. Using confocal microscopy to visualize organelle colocalization, the efficient and reversible induction of mitochondria-lysosome contacts is shown with the abscisic-acid-responsive system. Findings indicate that mitochondrial constructs tagged with mCherry and iRFP effectively mediate abscisic-acid-induced mitochondria-lysosome colocalization when paired with lysosomal constructs tagged with EGFP/BFP or lacking a fluorescent tag. In live-cell imaging experiments, mitochondria-lysosome contact durations are tunable with this system, increasing proportionally with abscisic-acid concentration used. Overall, the system of abscisic-acid-induced reversible organelle interactions is positioned as a powerful biological tool for studying organelle dynamics and membrane contact sites functions, with relevance to therapeutic strategies in neurodegenerative disorders and organelle dysfunction.

INTRODUCTION

Membrane contact sites (MCS) are areas of close proximity between two membrane-bound organelles that fulfill a specific function and that are distinct from incidental membrane association or fusion events. The involvement of organelle contacts has been implicated in a variety of cellular functions, including organelle fission, trafficking, and cellular metabolism. Importantly, misregulation of MCS is a feature of several neurodegenerative diseases, though the precise contribution of disrupted MCS to disease pathology remains an important question.[1,2] While the scientific field realizes the significance of studying organelle contacts, developing effective molecular tools to probe their functions remains a limitation. In this paper, the design of a biosynthetic system that can be used to study MCS function via the reversible induction of mitochondria-lysosome contacts is presented.

Mitochondria are sites of essential cellular processes such as adenosine triphosphate production, oxidative phosphorylation, apoptosis, calcium homeostasis, and lipid storage, which makes them central sites of cellular metabolism.[3] Mitochondrial dysfunction and dysregulation are also

hallmarks of aging, neurodegeneration, cardiovascular problems, and even cancer.[4] Likewise, lysosomes are versatile organelles critical to metabolic regulation and cell homeostasis.[5] They are prominently understood to function in the recycling of proteins and lipids, but an underappreciated functional corollary is their role in storing metabolites and signaling nutrient status to the cell in order to direct metabolic programming.[6,7] Importantly, impairment of normal lysosomal function is oftentimes associated with neurodegenerative diseases.[8,9]

Mitochondria-lysosomal contacts are more transient than other organelle contacts, but they still share similar characteristics, such as metabolite transfer and dedicated tether proteins.[10,11] Recent research suggests that mitochondria-lysosomal contacts play an important role in the regulation of localized protein synthesis in neurons, which raises the importance of this type of organelle contact in the context of neurodegenerative disease and pathology.[1] In particular, genes associated with Parkinson's disease (PD) appear to cluster around mitochondrial and lysosomal processes, and mitochondria-lysosomal contacts are often disrupted by mutations in these genes, which suggests that the crosstalk between mitochondria and lysosomes may feature prominently in PD pathogenesis.[12]

Many biological techniques have been used to characterize and study membrane contact sites. The most popular used in MCS studies are electron microscopy (EM), proximity ligation assay (PLA), live-cell confocal microscopy, and single molecule imaging involving fluorescence resonance energy transfer (FRET), or structured illumination microscopy (SIM).[13,14] These techniques have unique advantages in the study of MCS, however, each technique faces limitations. For example, SIM, FRET, and live-cell confocal microscopy can be used on live samples but demand specialized equipment, while EM and PLA require tissue fixation and dehydration procedures that may disrupt the original architecture of the contact sites, which in turn prevents the study of dynamics and function in living cells. Moreover, to examine the causal effect of contacts on other cellular functions, there is a need for a biological system that will allow us to directly manipulate the induction of mitochondria-lysosome contacts instead of passively observing them. This issue is addressed by proposing a biosynthetic inducible system of reversible organelle interactions, where the small molecule abscisic acid (ABA) is used as a mediator of mitochondria-lysosome colocalization.

ABA is a plant stress hormone that mediates heterodimeric complexation of proteins containing ABI (ABA insensitive 1) and PYL (pyrabactin resistance-like) domains.[15] To induce colocalization between mitochondria and lysosomes, protein constructs were engineered on the membranes of each organelle to include these compatible domains. Fluorescent protein tags were included to visualize mitochondria-lysosome colocalization via confocal microscopy. Interactions between organelles were induced by introducing ABA to cells that express these domains on the organelle membranes. Organelle contact was reversed via washout of ABA from the cells to relax the association of heterodimer complex. Different mitochondrial and lysosomal membrane construct variants are tested to identify more compatible pairs with additional biological assays.

METHODS

Plasmids

The plasmids were designed and cloned manually. Addgene Plasmid #171013 was used as a backbone for designing each plasmid. Plasmids were designed that contained the following coding sequences: 3xMyc-PYL-mCherry; 3xMyc-PYL-iRFP; 3xMyc-PYL; TMEM192-ABI-EGFP-3xHA; TMEM192-ABI-BFP-3xHA; and TMEM192-ABI-3xHA.

Cloning of constructs

ABI and PYL domain sequences were generated by synthetic gene fragment synthesis, featuring mammalian codon optimization of the domains present in Addgene plasmid #38247. Lentiviral plasmids containing the mitochondria and lysosomal targeting domains were linearized by restriction digestion of Addgene plasmid 171013 in-frame with the targeting domains. Polymerase chain reaction (PCR) was used to generate products containing the ABI/PYL domains and products containing fluorophores and epitope tags. Primers in these PCR reactions were designed to have overlapping homology regions. Then, Gibson ligation reactions were used to combine PCR reactions into the digested backbones. Finally, plasmids were transformed into E. coli and individual bacterial clones were screened for successfully combined plasmids, which were then purified from bacterial DNA preparations for preparation of lentivirus.

Transfection of lysosomal and mitochondrial plasmids

Lentivirus generation and a stable transduction of constructs into HeLa cells was performed.

Cell culture and passaging of HeLa cells

Cells were regularly passaged to maintain log-phase growth in FBS-supplemented DMEM. When cells were nearly confluent, they were passaged with trypsin to lift and separate cells from the surface of the dish to which they were adhered, then the cells were pelleted in a centrifuge, resuspended in DMEM, and appropriate dilutions of cells were added to a fresh plate.

Treatment with abscisic acid and mitochondrial stressors

After aspirating old cell culture media, new media with either 1 μM, 500 nM, or 300 nM ABA was added to the cells. HeLa cells were then incubated for 90 minutes in the course of one ABA treatment. For treatment of HeLa cells with mitochondrial stressors, the following drug concentrations were used with their respective incubation times: 5 μM MitoParaquat for 60 minutes, 5 μM Rotenone for 90 minutes, 5 μM Oligomycin for 120 minutes, 5 μM CCCP for 150 minutes, and 5 μM Antimycin A for 180 minutes.

Immunoblotting

Proteins from cell lysates were prepared and resolved in 4-20% SDS-PAGE gradient gel at 140V for 1 hour and transferred on a PVDF membrane for 15 minutes via semi-dry transfer. Membranes were blocked with 1% BSA-TBST for 1 hour. Primary antibody stain was applied in 1% BSA-TBST and membranes were incubated overnight at 4C. The following primary antibodies and concentrations were used: 1:500 of HA (Rb, Cell Sig. 3724S), and 1:1000 of Myc (Rb, Cell Sig. 2272S). Membranes were then washed 4 times for 20 minutes total with TBST solution and incubated with 1:10,000 of Goat anti-Rabbit HRP (Jackson 115-035-144) secondary antibody for 1 hour in 1% BSA-TBST. The membranes were washed again 4 times for 20 minutes total with TBST solution and stored in DI water until they were imaged with horseradish peroxidase substrate. Images were edited using FIJI image analysis software.

Immunofluorescence

In preparation for immunofluorescence, cells were grown on number 1.5 thickness slide covers. After corresponding ABA treatment, media was aspirated from all samples and formaldehyde was added to each sample. Samples were then washed with PBS and transferred into the blocking solution for 30 minutes. Afterwards, samples were treated with 1:500 of HA (Rb, Cells Sig. 3724S) and 1:500 Myc (Mo, Cell Sig. 2276S) as primary antibodies and incubated at room temperature for 1 hour. Next, samples were washed with PBS again, treated with 1:1000 of Rb-488 (Invitrogen A21206 or A11034) and 1:1000 of Mo-568 (Invitrogen A11031) secondary antibodies, and incubated at room temperature for 30 minutes. Samples were washed with PBS again, inverted, and adhered to slides with liquid mountant.

Confocal Microscopy

Microscopy was performed using a Nikon AXR confocal microscope with a 4-laser system (408, 488, 561, 640 nm), with corresponding emission filters and multispectral detectors. The system was equipped with PerfectFocus system and CO2 and a heat-controlled Tokai Hit chamber for live-cell imaging. Nikon elements imaging software was used. Image analysis was conducted using Cell Profiler and FIJI ImageJ. ANOVA p-test with post hoc Tukey test were conducted to determine significance between signal reading before ABA treatment, with ABA treatment, and after washout of ABA.

Live Cell Microscopy

Imaging parameters were 1024x1024 pixels, encompassing a space of 73.66 um by 73.66 um. This calculates to a resolution of 72 nm per pixel, though the true resolution limit for conventional light microscopy is ~200 nm. Image series were taken at 3 second intervals over a span of 3 minutes, for a total of 61 images per times series. Over the course of imaging, 5% CO_2 and 37°C were maintained. Post-hoc, 1 nm radius rolling-ball method background subtraction was applied using FIJI to facilitate analysis. Blinded analysis was performed on the images. During image series analysis, any lysosomal fluorescence signal that completely overlapped or visually touched the surface of mitochondrial signal on the first image in the series was considered to be in contact with mitochondria. Next, the proximity of such lysosomes with mitochondria was tracked with each consecutive image. When a tracked lysosome dissociated from mitochondrial signal and proceeded to move away for more than 2 images (6 seconds), the number of the last image that featured mitochondrial-lysosomal contact was recorded as the duration of contact in seconds. About 15 lysosomes per image series were tracked for contact duration in different locations inside a given cell.

RESULTS

In the initial design of the inducible system for mitochondria-lysosome interactions, lysosomal transmembrane protein 192 (TMEM192) was modified with C-terminal fusion of an ABI domain, a green fluorescent protein (EGFP), and triplicate HA epitope tag (for antibody-based recognition). Additionally, the transmembrane domain of the mitochondrial protein SYNJ2BP was modified with N-terminal fusion of the fluorescent protein mCherry, the PYL domain, and a triplicate Myc epitope tag (Figure 1A). When HeLa cells expressing these constructs are treated with ABA, ABA links ABI and PYL domains together, which forms a synthetic tether between the two organelles. To test if this interaction is enough to induce mitochondria-lysosome contacts in human cells, confocal microscopy and immunofluorescence were used to measure the colocalization between mitochondria and lysosomes.

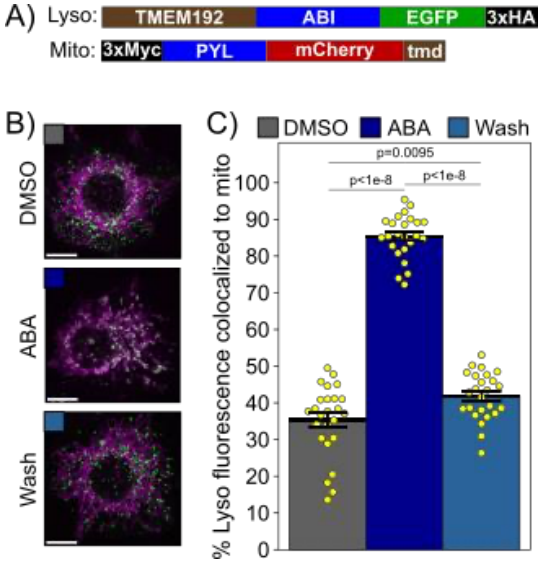

Figure 1. A system to reversibly induce mitochondria-lysosome contacts.

A) ABA mitochondrial and lysosomal heterodimer constructs. ABI/PYL are the ABA responsive domains; tmd – SYNJ2BP trans-membrane domain.

B) Fluorescence microscopy imaging of construct colocalization in HeLa cells with or without 1 μM ABA.

C) Quantification of mitochondria-lysosome association in individual cells for each treatment. Scale bars in (B) are 10 μm. ABA treatment duration is 30 minutes, and the duration of the washout is 90 minutes.

To test the system, HeLa cells expressing mitochondrial and lysosomal constructs were treated with DMSO (null treatment) or 1 μM ABA, followed by fixation of the samples. Fluorescence microscopy protocols were implemented to image fluorescence signals from lysosomes and mitochondria. The percentage of lysosomal fluorescence intensity was quantified in pixels of overlapping mitochondrial and lysosomal signal to define the extent of mitochondria-lysosome colocalization. While organelles contacts are classically defined as distances (10-80 nm) below the resolution limit of conventional light microscopy (~200 nm), the protein heterodimerization mediated by ABA would indeed tether the two organelles at distances within the classically defined range.[2] Thus, while not an absolute measure of contacts, changes in mitochondria-lysosome colocalization due to ABA treatment will strongly correlate with changes in contacts (Figure 1A).

Under baseline conditions, such as when HeLa cells are treated with DMSO control, only some lysosomes colocalized with mitochondria. However, treatment of cells with 1μM ABA was visually striking, with lysosomes colocalizing with the mitochondrial membrane to produce pixels of vivid, bright white overlap between fluorescent signals (Figure 1B). When ABA is washed out, the cells returned to baseline distribution of the organelles, with most lysosomes dissociated from mitochondria (Figure 1B). After quantifying mitochondria-lysosome colocalization, only 35% of the lysosomal intensity colocalized with mitochondria in DMSO (Figure 1C). Upon 1μM ABA treatment, the extent of mitochondria-lysosome colocalization significantly increased to 85%, consistent with qualitative observations. This substantial increase in colocalization suggests a strong inducible effect of the ABI-PYL domain system. The colocalization percentage returned to 40% after washing out ABA, indicating the reversibility of contact induction with ABA. Significant statistical differences were found between the colocalization signals in each group (Figure 1B), which confirms that colocalization between two organelles was induced and reversed after ABA wash-out. These results demonstrate that the ABI-PYL heterodimer works well for inducing and reversing proximity between organelle membranes expressing these domains.

After the system was seen for reversible organelle contacts working with EGFP-tagged lysosomes and mCherry-tagged mitochondria, the next question was what other fluorescent protein pairs can effectively visualize

mitochondria-lysosome colocalization. EGFP and mCherry are among the brightest and most stable fluorophores and are thus suitable choices for experiments in which only lysosomes and/or mitochondria are being imaged. However, other biological assays, such as those which measure mitochondrial reactive oxidant species (ROS), mitochondrial membrane potential, or lysosomal pH, often feature red or green fluorescent probes. These probes usually have significant spectral overlaps with EGFP and mCherry, requiring use of alternative fluorophores to visualize these probes simultaneously with the lysosomal and mitochondrial protein constructs. Hence, further investigation focused on identifying fluorophore tags that would be effective for contact induction with the ABA-induced system and compatible with assays that use green or red fluorescent indicators.

Mitochondrial mCherry construct performance was compared to the same construct lacking the mCherry fluorophore and the construct with infra-red fluorescent protein (iRFP670 or “iRFP”) instead of mCherry.

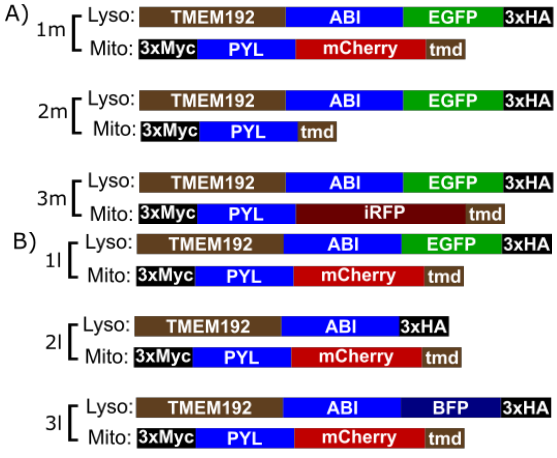

Figure 2. Mitochondrial and lysosomal variants.

A) Constructs of PYL with mCherry/no-FP/iRFP on mitochondrial tmd, paired to lysosomal construct with ABI and EGFP.

B) Constructs of ABI with EGFP/no-FP/BFP on lysosomal TMEM192PYL, paired to mitochondrial construct with PYL and mCherry.

An additional aim was to determine if there would be an advantage in removing EGFP from the lysosomal membrane construct and if blue fluorescent protein BFP would provide a similarly effective signal to EGFP. Hence, six constructs with different fluorescent protein tags on mitochondrial and lysosomal membranes were design. The following combinations of fluorophore tags were tested: lysosomal-EGFP against mitochondrial-mCherry/no-FP (no-fluorescent protein)/iRFP as well as mitochondrial-mCherry with lysosomal EGFP/no-FP/BFP (Figure 2A construct pairs 1m, 2m, 3m; Figure 2B construct pairs 1l, 2l, 3l).

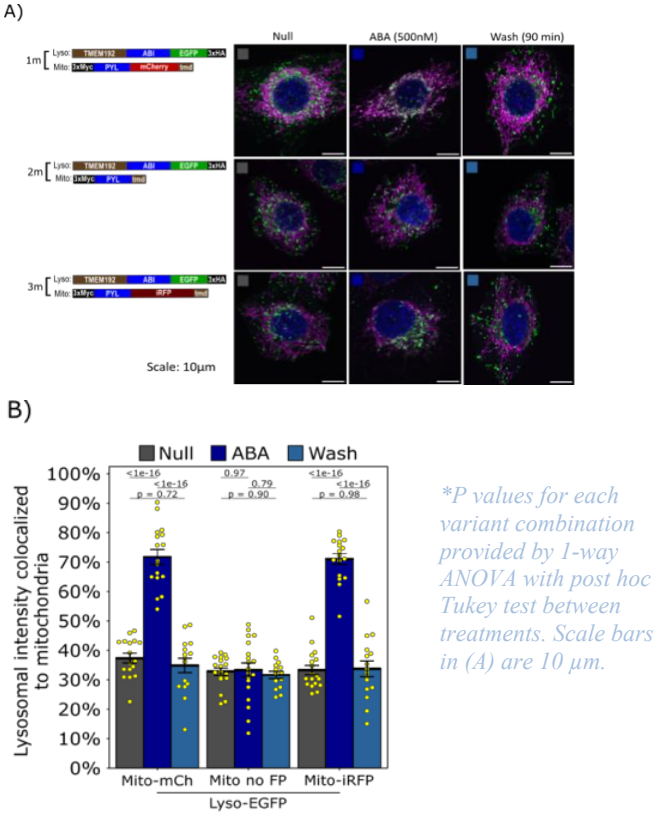

**P values for each variant combination provided by 1-way ANOVA with post hoc Tukey test between treatments. Scale bars in (A) are 10 µm.*

Figure 3. Testing ABA-induced lysosome-mitochondria colocalization of mitochondrial construct variants.

A) Immunofluorescent imaging of construct colocalization in HeLa cells with or without 30-minute treatment of 500 nM ABA.

B) Quantification of mitochondria-lysosome association in individual cells.

HeLa cells that expressed the different combinations of construct pairs were treated with 500 nM ABA or DMSO (null treatment) for 30 minutes before fixation or with ABA treatment and 90 minutes of washout before fixation (Figure 3A). Lysosomal colocalization was quantified for each treatment (Figure 3B). To keep quantification consistent across samples, immunofluorescence was performed against the HA and Myc tags present in each construct, rather than taking the direct measurement of the fluorophores. Constructs expressing mitochondrial mCherry and iRFP (Figure 3A, construct pairs 1m and 3m respectively) produced the same profile of induced and reversible contacts. On microscopy images, HeLa cells were seen expressing both 1m and 3m construct pairs showed a similar lysosomal colocalization to mitochondria upon ABA treatment and the same relaxation of contacts after the washout (Figure 3A, construct pairs 1m and 3m), which correlates with an increase in organelle colocalization from 40% to 70% (Figure 3B, Mito-mCh and Mito-iRFP). Similarly, both construct variants exhibited return of mitochondria-lysosome colocalization to the baseline of about 40% colocalization (Figure 3B, Mito-mCh and Mito-iRFP). In contrast, it appears that cells expressing mitochondrial no-FP variant were unable to mediate mitochondria-lysosome contact induction, as there are no lysosomes colocalizing with the mitochondria upon ABA treatment on microscopy (Figure 3A, construct pair 2m). Furthermore, there is no change in extent of colocalization qualitatively (Figure 3B, Mito no-FP). It is possible that removing the fluorophore from the mitochondrial construct variant situates the PYL domain too close to the mitochondrial membrane which sterically impedes the ABI-PYL complex from forming. This leads to absence of contact induction upon ABA treatment.

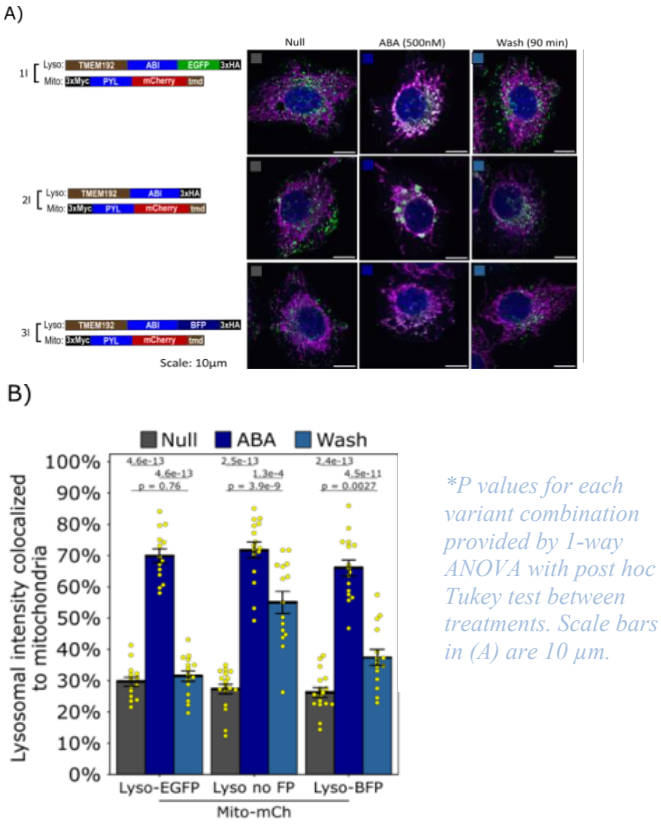

*P values for each variant combination provided by 1-way ANOVA with post hoc Tukey test between treatments. Scale bars in (A) are 10 µm.

Figure 4. Testing ABA-induced lysosome-mitochondria colocalization of lysosomal construct variants.

A) Immunofluorescent imaging of construct colocalization in HeLa cells with or without 30-minute treatment of 500 nM ABA.

B) Quantification of mitochondria-lysosome association in individual cells for each construct combination in each treatment.

A similar approach was taken to test HeLa cells expressing varying lysosomal constructs. Cells expressing all lysosomal EGFP, no-FP, and BFP constructs produced visually the same contact induction profile with 70% mitochondria-lysosome colocalization (Figure 4). After ABA treatment, cells expressing the lysosomal no-FP construct variant showed increased mitochondria-lysosome colocalization, but most lysosomes remained in contact with mitochondria after the washout with about 55% colocalization post-wash compared to EGFP baseline value of 30% (Figure 4A construct pair 2l, Figure 4B Lyso no-FP,

Lyso EGFP). As expected, The design of the the lysosomal no-FP construct did not change the distance between ABI and the organelle membrane (Figure 2A, construct pair 2l). Thus, in this case, removing the fluorophore should not have had as strong of an impact on contact induction as in the case of the mitochondrial no-FP construct. Interestingly, changes in lysosomal morphology were present during contact induction in cells expressing lysosomal no-FP construct, where lysosomes clustered more in cells expressing lysosomal no-FP construct than in cells expressing other constructs (Figure 4A, construct pair 2l). The lack of fluorophore in the lysosomal construct may allow for tighter packing of the heterodimer complex, which could explain this morphological change as well as the reduced recovery after washout. Some lysosomes remained in contact with mitochondria post-washout in cells expressing lysosomal BFP (Figure 4A, construct pair 3l), which correlated with a slightly diminished post-washout lysosomal colocalization of about 40% (Figure 4B, Lyso BFP).

If a construct variant is expressed at a higher level, there may be increased binding opportunities at contact sites, leading to more stable tethers that make relaxation of contacts upon ABA washout more difficult. Thus, it was hypothesized that differences in expression levels of the heterodimer constructs might underlie small differences in the reduction of mitochondria-lysosome colocalization after washout. To address this question, immunoblotting on the whole-cell lysate of the HeLa cell lines expressing the construct variants was performed. Toward this end, blotting was carried out for the lysosomal HA and mitochondrial Myc tags, incorporated in the lysosomal and mitochondrial construct designs (Figure 2, Figure 5). Cell lines with lysosomal-EGFP and a mitochondrial variant had similar HA expression across construct variants.

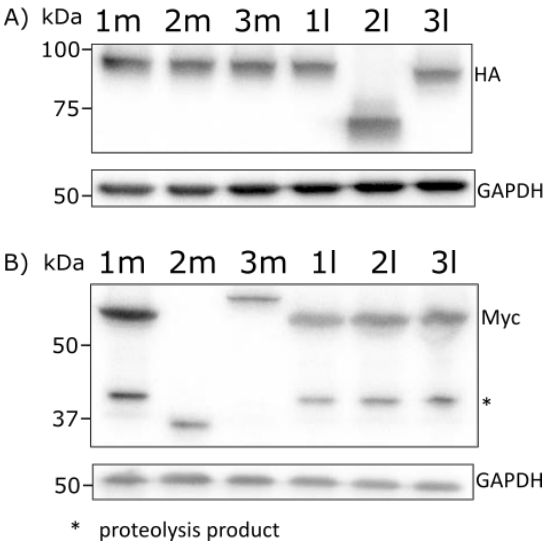

Figure 5. Immunoblotting of the whole-cell lysate to examine construct level expression.

*Western blots against HA (A) and Myc (B) in whole-cell lysate of HeLa cells expressing tested construct variants. Proteolysis product is indicated with an asterisk * and the band in 2m line (B) is a full length and a lower weight construct variant product, but not a proteolysis product. This data is a result of a single immunoblotting experiment (n=1).*

However, Myc expression levels were lower in cells with 2m construct, which correlates with the lack of contact induction in 2m cells observed during microscopy experiments (Figure 3B, Mito no FP). In cell lines with mitochondrial mCherry and a lysosomal variant, there were similar HA expression across all lysates. There was a higher Myc expression in cells with 2l and 3l construct pair variants, which aligns with reduced washout efficiency in cells with these constructs during microscopy (Figure 4B). These results suggest that the expression of the lysosomal construct is a limiting factor in the stability of the induced mitochondria-lysosome contacts in the ABA-directed system. As the immunoblotting data was derived from a single experiment, further replicates are required to draw definitive conclusions.

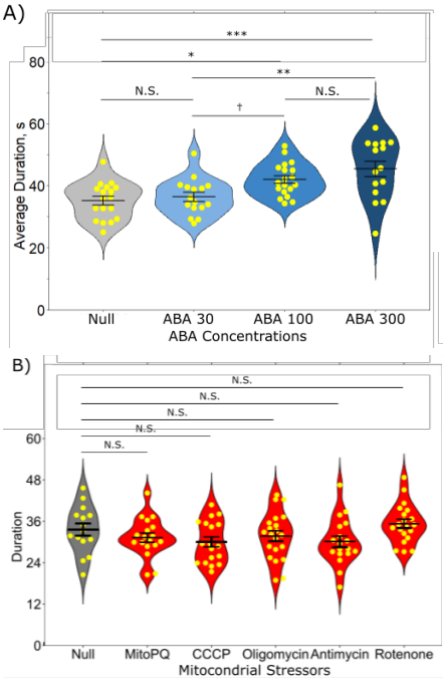

** P values are provided by 1-way ANOVA with post hoc Tukey test between treatments.*

P values are provided by Dunnett's test (95% family-wise confidence level). "*" $p < 0.001$, "**" $p < 0.01$, "*" $p < 0.05$, "†" $p < 0.1$,*

Figure 6: Quantification of mitochondria-lysosome contact duration.

A) Average contact durations when HeLa cells are treated with 0 nM, 30 nM, 100 nM, and 300 nM ABA.

B) Average contact durations when HeLa are treated with MitoPQ, CCCP, Oligomycin, Antimycin A, and Rotenone.

After extensively testing ABA as a tool to induce mitochondria-lysosome contacts, this system was used to assess whether the extent of contact induction could be modulated by varying the concentration of ABA. In addition to quantifying lysosome-mitochondria overlap, the contact duration is another important measure for defining the in-duction of bona fide organelle contacts.[10] Organelle contacts are highly dynamic processes that involve multiple native or artificial tethers, such as the ones induced with ABA. Thus, the duration of organelle contacts reflects the equilibrium of the number of active tethers, which are expected to increase with increasing ABA. To test this hypothesis, HeLa cells were transduced with mito-mCherry/lyso-EGFP constructs and treated with ABA. There were statistically significant increases in average contact duration in cells treated with increasing ABA concentrations (Figure 6A). These results confirm that it is possible to tune the extent of contact induction in ABA-induced systems by manipulating abscisic acid concentrations.

In addition to studying induced mitochondria-lysosome contacts, the fluorophores on mitochondria and lysosome construct pairs can be used to track changes in contacts produced by other sources of cellular stress. Live cell imaging and contact quantification were used explore the effect of mitochondrial stressors on the duration of mitochondria-lysosome contacts. Altered contacts induced by these stressors could be indicators of cellular responses involving lysosomes, such as calcium exchange, metabolite transfer, or quality control of damaged proteins or membranes. Cells were treated with five drugs (mi-to-paraquat, CCCP, oligomycin, antimycin A, and rotenone) that induce mitochondrial stress through various mechanisms. Contact duration in each treatment averaged close to 100 seconds, but there was no statistically significant differences between null treatment and mitochondrial stressors with respect to contact duration (Figure 6B).
None of mitoparaquat, CCCP, oligomycin, antimycin A, or rotenone have any effect on the duration of mitochondria-lysosome contact duration at the concentrations and treatment times.

DISCUSSION

The system for ABA-mediated heterodimerization represents a novel tool for the reversible induction of organelle contacts. In immunofluorescence and live-cell confocal microscopy imaging, the system demonstrated tunable control of mitochondria-lysosome contacts, representing a powerful biosynthetic tool for studying dynamic organelle interactions in human cells.

To maximize the applicability of this tool, it was investigated whether it was compatible

with various fluorescent protein tags. mCherry and iRFP as mitochondrial tags were found to be equally effective for visualizing organelle colocalization in the ABA-induced system. Additionally, BFP in the lysosomal construct shows comparable results to EGFP, suggesting that the fluorescent protein tag on each construct can be altered without sacrificing the efficacy of reversible organelle contact induction. While the lysosomal construct could also tolerate the removal of the fluorescent protein tag, excision of the mitochondrial fluorophore tag abolished ABA-inducible contact formation. This may be due to steric effects from shortening the distance between the transmembrane and PYL dimerization domains. Optimizing geometric parameters of constructs, such as lengths of linker regions between functional domains, is an important aspect of protein engineering. With additional design iteration, it should be possible to generate a mitochondrial construct without fluorophores that properly mediates organelle contacts in the presence of ABA.

The immunoblotting experiments highlighted that the extent of contact formation between organelles shows some dependence on expression levels of the protein constructs, especially regarding changes in the lysosomal construct organization. Additionally, increasing ABA doses highlighted the tunability of the system. Knowing that contact levels and their duration can be directly manipulated by changing abscisic acid dosage can be useful in future experiments that aim to balance the effect size of other genetic tools or chemical perturbations to mitochondria-lysosome contacts.

While the investigation into the effect of mitochondrial stress on contact duration did not yield positive results, there is no definitive conclusion that mitochondrial stress does not affect mitochondria-lysosome contact induction. The drugs used in the experiment induced mitochondrial stress via disruption of the electron transport chain (ETC) activity or by generating reactive oxidant species. Additional types of mitochondrial stress, along with different dosages and treatment durations, should be investigated in the future to study their effect on mitochondria-lysosome contact induction. Future studies could investigate how lysosomal stress influences the formation of mitochondria–lysosome contacts, as it remains unclear which organelle provides the primary signal initiating this interaction.

CONCLUSION

In this study, ABA-responsive heterodimerization was demonstrated to be an effective biosynthetic approach to induce reversible mitochondria-lysosome interactions. Data indicates that the developed system is quantifiable and modular with respect to the choice of fluorophore tags.

Substantial significance is emphasized because the ability to manipulate organelle proximity through the ABI-PYL system provides new ways to investigate the functional roles of mitochondria-lysosome contacts. Developing effective molecular proximity tools for MCS detection is an ongoing challenge in the field and has limited the ability to examine the effects of these contacts on organelle dynamics and metabolic processes. By providing means to induce and reverse interactions dynamically, the system offers a valuable model to test hypotheses about how these organelles communicate in normal physiological function or in the context of disease. Importantly, although only the induction of mitochondria-lysosome contacts was demonstrated, the paradigm of ABI-PYL membrane protein heterodimers should be applicable to studies of other organelle contacts.

The impaired function of mitochondria and lysosomes have been studied separately from each other for a long time in the context of

neurodegenerative diseases like PD, Charcot-Marie-Tooth disease, and others. However, it is becoming increasingly clear that processes that emerge from their dynamic association must be studied.[1] Thus, tools like the presented ABA-induced system for reversible mitochondria-lysosome contacts provide new avenues for investigating the pathology of these disorders. With additional engineering, the design of ABA-induced protein heterodimer formation can also be modified to study contact sites of other organelles. In the context of neurodegeneration, recent literature highlights the importance of exploring ER-mitochondria, ER-endolysosome, ER-plasma membrane, and ER-lipid droplet interactions.[14] More research will be performed to elucidate the applicability of the ABA-induced system to these types of MCS.

To study the function of mitochondria-lysosome association in the context of PD, it would be helpful to apply this system in iPSC-derived dopaminergic neurons—a cell line more relevant to Parkison's. To do this, CRISPR donor plasmids for each of the constructs are being designed. These plasmids will leverage the gene-editing technology of CRISPR to integrate the constructs into iPSC lines, including those of individuals with PD-causal mutations, allowing for the identification of which PD-associated genes are impacted by alterations to mitochondria-lysosome contacts. This integrated approach may shed light on cell type-specific molecular mechanisms of neurodegeneration and could lead to the development of new or targeted therapeutic strategies.

AUTHOR INFORMATION

Corresponding Author

Yuliia Kohut – ykohu@illinois.edu

Author Contributions

Yuliia Kohut performed microscopy, immunoblotting, cloning experiments, and data analysis. She also wrote the manuscript and generated most of the figures. Dr. Robert Coukos provided guidance and direction on conceiving and performing experiments during the project, including editing the manuscript. He also performed transfection of HeLa cells with lentivirus, cell culture work, and live-cell imaging. Dr. Dimitri Krainc also provided direction and support during the project.

Abbreviations

ABA - Abscisic acid

ABI - ABA insensitive 1

BFP - Blue fluorescent protein

CRISPR - Clustered regularly interspaced short palindromic repeats

EGFP - Extra green fluorescent protein

EM - Electron microscopy

ER - Endoplasmic reticulum

FRET - Fluorescence resonance energy transfer

iPSC - Induced pluripotent stem cells

iRFP - Infra-red fluorescent protein

MCS - Membrane contact sites

no-FP - No-fluorescent protein

PCR - Polymerase chain reaction

PLA – Proximity ligation assay

PYL - Pyrabactin resistance-like

SIM - Structured illumination microscopy

TMEM192 - Transmembrane protein 192

tmd - SYNJ2BP transmembrane domain

REFERENCES

[1] Kim S, Coukos R, Gao F, Krainc D (2022) Dysregulation of organelle membrane contact sites in neurological diseases. Neuron 110(15):2386–2408.

[2] Scorrano L, et al. (2019) Coming together to define membrane contact sites. Nature Communications 10(1). doi:10.1038/s41467-019-09253-3.

[3] Chen W, Zhao H, Li Y (2023) Mitochondrial dynamics in health and disease: Mechanisms and potential targets. Signal Transduction and Targeted Therapy 8(1). doi:10.1038/s41392-023-01547-9.

[4] Li Y, Berliocchi L, Li Z, Rasmussen LJ (2023) Interactions between mitochondrial dysfunction and other hallmarks of aging: Paving a path to-ward interventions that promote healthy old age. Aging Cell 23(1). doi:10.1111/acel.13942.

[5] Trivedi PC, Bartlett JJ, Pulinilkunnil T (2020) Lysosomal Biology and function: Modern view of cellular debris bin. Cells 9(5):1131.

[6] Bonam SR, Wang F, Muller S (2019) Lysosomes as a therapeutic target. Nature Reviews Drug Discovery 18(12):923–948.

[7] Lamming DW, Bar-Peled L (2018) Lysosome: The Metabolic Signaling Hub. Traffic 20(1):27–38.

[8] Udayar V, Chen Y, Sidransky E, Jagasia R (2022) Lysosomal dysfunction in neurodegeneration: Emerging concepts and methods. Trends in Neurosciences 45(3):184–199.

[9] Ysselstein D, Shulman JM, Krainc D (2019) Emerging links between pediatric lysosomal storage diseases and adult parkinsonism. Movement Disorders 34(5):614–624.

[10] Wong YC, Ysselstein D, Krainc D (2018) Mitochondria–lysosome contacts regulate mitochondrial fission via Rab7 GTP hydrolysis. Nature 554(7692):382–386.

[11]

[12] Wong YC, Ysselstein D, Krainc D (2018) Mitochondria–lysosome contacts regulate mitochondrial fission via Rab7 GTP hydrolysis. Nature 554(7692):382–386.

[13]

[14] 11. Cantarero L, et al. (2020) Mitochondria–lysosome membrane contacts are defective in GDAP1-related Charcot–Marie–Tooth disease. Human Molecular Genetics 29(22):3589–3605.

[15] 12. Coukos R, Krainc D (2024) Key genes and convergent pathogenic mechanisms in Parkinson disease. Nature Reviews Neuroscience 25(6):393–413.

[16] 13. Huang X, Jiang C, Yu L, Yang A (2020) Cur-rent and emerging approaches for studying inter-organelle membrane contact sites. Frontiers in Cell and Developmental Biology 8. doi:10.3389/fcell.2020.00195.

[17] 14. Gamuyao R, Chang C-L (2024) Imaging and proteomics toolkits for studying organelle con-tact sites. Frontiers in Cell and Developmental Biology 12. doi:10.3389/fcell.2024.1466915.

[18] Liang F-S, Ho WQ, Crabtree GR (2011) Engineering the ABA plant stress pathway for regulation of induced proximity. Science Signaling 4(164). doi:10.1126/scisignal.2001449.

CUSJ
COLUMBIA UNDERGRADUATE SCIENCE JOURNAL

Unveiling Dark Matter in a Galaxy: A Case Study of NGC 1068

Seonyu Lee[1], Heeju Kim[1]
[1]Department of Physics and Astronomy, Seoul National University, Seoul, Republic of Korea

KEYWORDS: Dark matter distribution, SED fitting, galaxy photometry

ABSTRACT: The dark matter distribution in NGC 1068 is analyzed by determining its mass using dynamical mass from HI-based rotation curves and stellar mass from spectral energy distribution fitting of ugriz photometric data. High-precision photometry was achieved through Gaussian fitting, star masking, 3-sigma clipping, and error propagation, enabling robust flux measurements for spectral energy distribution analysis with CIGALE. Beyond 1.5 kpc, the dynamical mass begins to exceed the stellar mass. As the error bars do not overlap, the presence of dark matter is confirmed. The difference between the two masses is used to map the dark matter distribution from 1.5 kpc to 13 kpc. This study reproduces earlier findings using high-resolution data. Furthermore, the method for constraining dark matter distributions in individual galaxies and provides detailed spectral energy distribution results with uncertainties is refined.

INTRODUCTION

In the 1930s, astronomer Zwicky introduced the concept of “dark matter”, a form of matter that interacts gravitationally but not with light, while studying the Coma Cluster.[1] Later in the 1970s, Vera Rubin confirmed the existence of dark matter by revealing the flatness of galactic rotation curves.[2] Despite accumulating evidence of dark matter’s existence, its nature remains one of the most significant unsolved mysteries in modern astrophysics.

Astrophysicists have studied dark matter’s distribution and interaction with baryonic matter within the cosmic environment, uncovering characteristics of dark matter particles. These studies have focused on large-scale structures such as galaxy clusters.[3,4,5] However, investigating dark matter distribution within individual galaxies is equally important, as it provides valuable insights into galaxy formation and evolution and the interaction between dark and baryonic matter.[6,7] Additionally, galaxy simulations under various dark matter models can help elucidate its nature.[8,9]

This study presents a method for determining the dark matter distribution within a single galaxy, using NGC 1068 as a case study. As a Seyfert Type 2 galaxy, NGC 1068 hosts a heavily obscured active galactic nucleus (AGN), making it a valuable target for studying the interplay between dark matter, stellar populations, and AGN activity. Its well-documented structure and abundant multi-wavelength data allow for a detailed investigation of both baryonic and non-baryonic components. By comparing gravitational mass derived from rotation curves with stellar mass from spectral energy distribution (SED) fitting, this study reproduces historical findings providing the existence of dark matter. Rotation curves probe the total gravitational potential of a

galaxy, while SED fitting constrains the stellar content based on photometry. Combining both enables us to isolate the dark matter component by comparing luminous and total mass distributions across different radii. Furthermore, it visualizes the radial distribution of dark matter within the galaxy.

For simplicity, the galaxy is modeled as a two-dimensional, axisymmetric plane. Although this ignores asymmetries, it helps us understand overall trends. Gravitational mass and its uncertainties are calculated from rotational curve data to map the gravitational mass distribution. Radial photometry is performed using optical filter FITS files, and photometric errors are calculated for SED fitting. The stellar mass and its uncertainty are derived from the best-fit parameters of the SED fitting process. These two methods collectively confirm the existence of dark matter, and the difference between the masses reveals the dark matter distribution, visualized as a colormap.

METHODS

Data

The observational data used in this study include FITS files of NGC 1068, captured with the ugriz filters using the LSGT at Siding Spring Observatory in Australia (Fig. 1). Additionally, the rotational curve data were employed, sourced from Brinks et al. (1997) [10]. This rotational curve consists of velocity measurements derived from HI emission lines et radii ranging from r = 20 arcsec to r = 180 arcsec (Fig. 2). The inclination of the galaxy is already corrected in the data, making this dataset well-suited for calculating the gravitational mass distribution across a broad radial range.

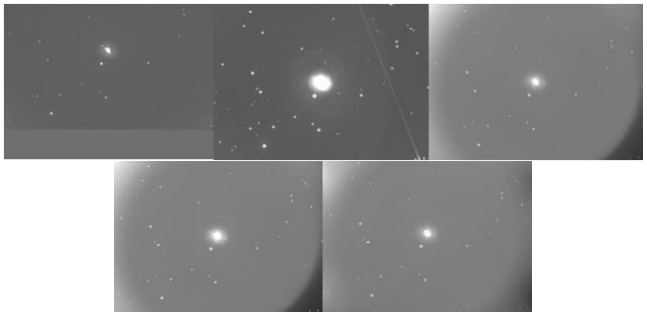

Figure 1. NGC 1068 imaged using ugriz filters with the LSGT.

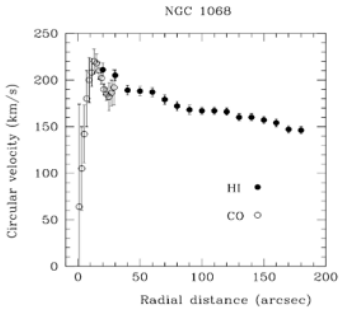

Figure 2. Rotation curve of NGC 1068.

Rotation curve

The rotation curve provides the distribution of velocities of stars and gas in a spiral galaxy as a function of radius, serving as a crucial tool for studying the galaxy's mass distribution and dynamics. From the rotation curve of NGC 1068 presented by Brinks et al. (1997), the velocities and their uncertainties were extracted at approximately 10 arcsecond intervals over the range r = 20 to 160 arcseconds.[10] Assuming a balance between centrifugal force and gravitational force according to Newtonian dynamics, the gravitational mass and its uncertainties were calculated using the following equation:

$$M = \frac{v^2 r}{G}, \qquad \frac{\Delta M}{M} = \frac{2\Delta v}{v}$$

SED fitting

SED fitting is a method used to optimize the flux emitted by galaxies across a broad range of wavelengths, from radio to X-ray. This technique provides insights into various physical properties of galaxies, such

as star formation rate, star formation history (SFH), stellar mass, attenuation, dust mass and properties, metallicity, and active galactic nuclei (AGN). As a critical tool in galaxy studies, SED fitting enables the estimation of galaxy evolution, activity, formation epochs, and the characteristics of stars and interstellar material within galaxies.[11,12,13,14]

The effectiveness of SED fitting can be enhanced through two primary approaches. The first is conducting observations across the widest possible range of wavelengths.[15] Different wavelength ranges predominantly trace distinct components of a galaxy. For instance, radio wavelengths trace AGNs and star formation, while infrared reveals emissions from gas, dust, and older stars. Optical wavelengths capture stellar light, and X-rays highlight AGNs and hot gas.[16,17,18,19] Observing galaxies across a comprehensive wavelength range thus facilitates more accurate SED fitting and modeling.

The second approach involves refining the models used for SED fitting.[20] Current SED fitting software incorporates models and modules that represent various components, such as SFH, single stellar population (SSP), nebular emission, dust attenuation, dust emission, and AGNs. By adjusting the types of modules and input parameters, the models can be tailored for greater accuracy.

The key steps in SED fitting are as follows:

1. Acquiring galaxy flux measurements through multi-wavelength photometry.
2. Setting up models and input parameters.
3. Performing fitting using statistical algorithms.
4. Outputting the optimized SED and corresponding physical parameters.

Among the physical parameters provided by SED fitting programs are stellar mass and its Bayesian uncertainties. In this study, we employed SED fitting to derive stellar mass and its associated errors from galaxy photometric data.

CIGALE

CIGALE, short for Code Investigating GALaxy Emission, is a software designed for performing SED fitting. As a Python-based program, CIGALE offers lower technical complexity compared to other SED fitting tools and improves user accessibility with its automated features.[21,22] It also allows high flexibility by enabling users to configure various modules and input parameters, as well as exclude unnecessary modules. Despite limited observational data, CIGALE outputs the best-fit SED and parameters through sophisticated statistical analyses, such as chi-square minimization and Bayesian inference. For these reasons, this study employed CIGALE for SED fitting.[20]

CIGALE includes a wide range of modules for SFH, SSP, nebular emission, dust attenuation, dust emission, AGN, X-ray, radio, and redshift. However, since the observational data in this study is limited to the ugriz filters and optical wavelengths, only modules relevant to stellar emission were selected. The modules used in this study are listed below:

1. SFH: sfhdelayed.[23]
2. SSP: bc03.[11]
3. Nebular emission: nebular.[24]
4. Dust attenuation: dustatt_modified_CF00.[25]

Modules related to dust emission, AGN, x-ray, and radio were excluded due to the absence of corresponding observational data. The selected modules for SFH, SSP, nebular emission, and dust attenuation were chosen to yield the most reliable results given the

limited dataset. Modules with fewer input parameters and simpler structures were prioritized. Input parameters for each module were configured by slightly expanding their default ranges.

The following steps summarize the workflow of CIGALE:

1. pcigale init: Create the config.ini file, which includes flux data for each filter, their measurement uncertainties, and module selections.
2. pcigale genconf: Configure the parameters for the selected modules.
3. pcigale check: Verify the parameter settings to ensure they are correctly configured before execution.
4. pcigale run: Generate all possible SED models based on the modules and parameters specified in config.ini, compare the models to the observed fluxes, select the model with the lowest chi-square value, and output the optimal SED model along with physical parameters.
5. pcigale-plots sed, pdf, chi2: Output graphs for the best-fit SED, parameter PDFs, and chi-square distributions.

CIGALE evaluates model fit quality and determines the optimal model using statistical techniques like chi-square minimization and Bayesian analysis. The chi-square computation incorporates a normalization factor for SFH, ensuring its integral equals one solar mass. This requires scaling the model values by a factor when calculating the chi-square.

$$\alpha = \frac{\sum_i \frac{f_i \times m_i}{\sigma_i^2}}{\sum_i \frac{m_i^2}{\sigma_i^2}} + \frac{\sum_j \frac{f_j \times m_j}{\sigma_j^2}}{\sum_j \frac{m_j^2}{\sigma_j^2}}$$

$$\chi^2 = \sum_i \left(\frac{f_i - \alpha \times m_i}{\sigma_i}\right)^2 + \sum_j \left(\frac{f_j - \alpha \times m_j}{\sigma_j}\right)^2 + \sum_k \left(\frac{f_k - m_k}{\sigma_k}\right)^2$$

Values with the subscript *i* represent the observed and model fluxes, while those with the subscript *j* denote observed and model parameters that depend on magnitude. Values with the subscript *k* correspond to observed and model parameters that are independent of magnitude. σ represents the observational uncertainties. CIGALE identifies the model with the smallest chi-squared value as the best-fit model and stores its corresponding SED graph and physical parameters in the results.fits and results.txt files.

While CIGALE identifies the optimal physical parameters by minimizing chi-square, galaxies with fundamentally different physical properties can exhibit similar SEDs. This issue becomes particularly challenging with limited observational data, as in this study.[20] To address this, CIGALE goes beyond parameter extraction by employing Bayesian analysis to derive probability distributions for each parameter. This process yields Bayesian mean values, Bayesian uncertainties, and confidence intervals for the parameters.

The Bayesian mean and confidence intervals are calculated using the following equations:

$$P(\Theta|D) = \frac{P(D|\Theta) \cdot P(\Theta)}{P(D)}$$

$$\langle \Theta \rangle = \frac{\int \Theta \cdot P(\Theta|D)\, d\Theta}{\int P(\Theta|D)\, d\Theta}$$

$$P(a \leq \Theta \leq b) = \int_a^b P(\Theta|D)\, d$$

Here, *D* represents the observational data, and θ represents the parameter of interest. In CIGALE's Bayesian framework, the likelihood

$P(\Theta|D)$ is weighted by the chi-square statistic.

$$P(D|\Theta) \propto e^{-\frac{1}{2}\chi^2}$$

Galaxy Photometry

After CIGALE input data required the redshift of NGC 1068, along with fluxes and their uncertainties in the ugriz filters at different radii. Since the initial values significantly impact CIGALE's results, accurate photometry and error estimation are essential. For NGC 1068, a redshift of z = 0.0038 was used.

Detecting the Center of the Galaxy

To identify the center of the galaxy, the surrounding stars and their associated background light were removed. This was achieved by averaging the brightness over small predefined regions and normalizing them to a uniform value. Subtracting the generated background from the original image resulted in a background-subtracted image. Additionally, excessively bright points were excluded to ensure accurate background estimation. This process was carried out using the photutils and astropy packages in Python.

The pixel coordinates with the maximum brightness were assumed to be the center of the galaxy. The brightness distribution was found to be sufficiently circularly symmetric based on the visualization of the galaxy's FITS file. Consequently, a 2D Gaussian fit was applied to model the peak in the symmetric distribution. The equation used for the Gaussian fitting is as follows:

$$f(x,y) = A \cdot \exp\left(-\left[\frac{(x-x_0)^2}{2\sigma_x^2} + \frac{(y-y_0)^2}{2\sigma_y^2}\right]\right) + C$$

The residual map indicated that pixel values near the center are close to zero (Fig. 3). These results verified the reliability of the Gaussian fitting, and the extracted coordinates were set as the center of the galaxy.

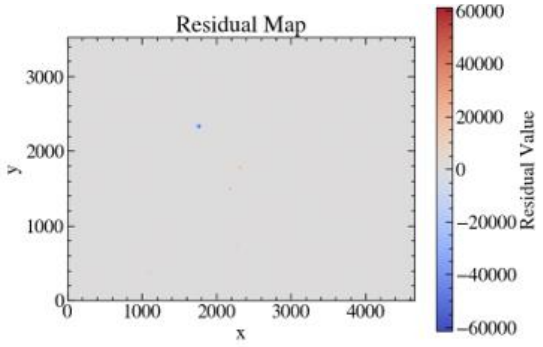

Figure 3. Residual map.

Masking star & radial photometry

To perform accurate photometry of the galaxy, bright stars within the aperture photometry region needed to be masked. Figure 4 shows the maximum photometry region used in this study and the masking of a bright star within that region. The center coordinates of the stars to be masked were identified, and the brightness of the detected star regions was replaced with pixel brightness corresponding to the background light.

The photometry radius was set to match the radii extracted from the rotation curve graph. As the galaxy was assumed to be circularly symmetric in this study, circular photometry was performed instead of elliptical photometry (Figure 5). The flux of the galaxy was calculated by summing the pixel brightness within the circular region and subtracting the background brightness times the area.

To convert the galaxy flux obtained in this manner into observational magnitudes, the following equation was used:

$$m = 22.5 - 2.5\log_{10}(F)$$

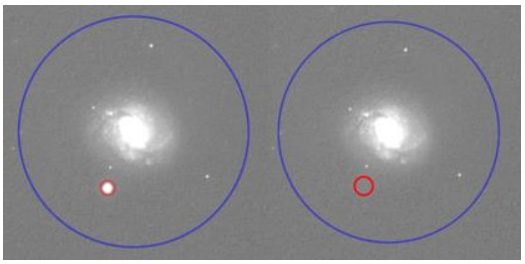

Figure 4. Stellar masking.

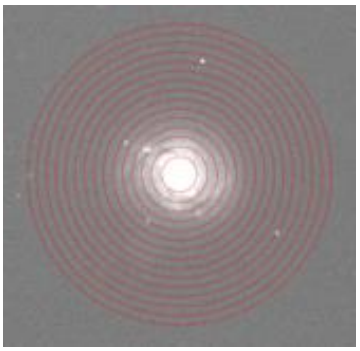

Figure 5. Radial circular photometry.

Secondary calibration

To derive the absolute flux from the observed data, standard stars within the dataset were identified. Their relative magnitudes were then compared to known absolute magnitudes to perform photometric calibration. However, the data in this study did not include standard stars. Thus, the right ascension (RA), declination (Dec), and relative magnitudes of stars were obtained and matched with SDSS data to determine absolute magnitudes (Figures 6, 7).[26]

Using the distribution of matched points, linear regression was applied to determine the values of *k* and ZP. To improve accuracy, outliers were removed using 3-sigma clipping (Figure 8). In 3-sigma clipping, points that deviate by more than three times the standard deviation from the distribution of other points are excluded. The equation used for this secondary calibration is as follows:

$$m_{\text{std}} - m_{\text{inst}} = k \cdot C_{\text{inst}} + \text{ZP}$$

$$C_{\text{inst}} = m_{i,\text{inst}} - m_{z,\text{inst}}$$

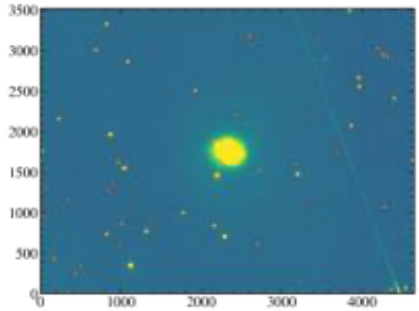

Figure 6. Star detection.

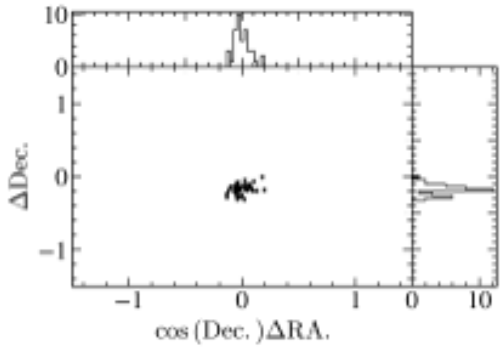

Figure 7. Matching errors in RA and Dec.

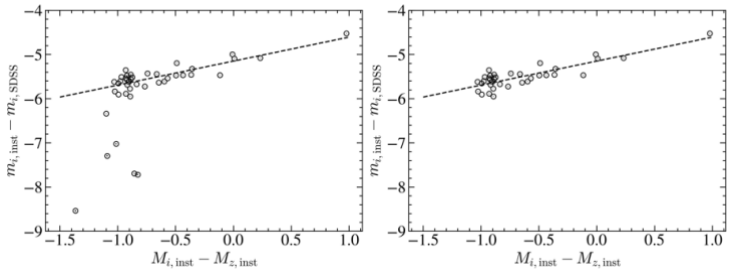

Figure 8. Before and after 3-sigma clipping.

Photometric error analysis

CIGALE requires input data in the form of fluxes and photometric uncertainties for each filter. The following equation was used to calculate magnitude uncertainties. The SNR represents the signal-to-noise ratio of the telescope, which was calculated assuming that the number of photons reaching the CCD follows a Poisson distribution.[27,28]

$$\text{SNR} = \frac{f_s}{\sqrt{f_s + f_{\text{bkg}}}}, \sigma_{m,\text{obj}} = \frac{2.5}{\ln(10) \cdot \text{SNR}}$$

The equation used to determine the uncertainty for secondary calibration is provided below.

$$\sigma_m = \sqrt{\left(\sigma_k (B-V)\right)^2 + (k\sigma_{B-V})^2 + \sigma_c^2 + \sigma_{m,\text{gal}}^2}$$

Lastly, the uncertainty arising from the process of converting absolute magnitudes into fluxes was calculated, with the value of f_0 set to $3.631*10^3$.

$$f = f_0 \cdot 10^{-0.4m}, \sigma_{\text{flux}} = \sigma_m \cdot 0.4 \ln(10) \cdot f$$

The final total uncertainty was determined by summing the squares of these individual

uncertainties and then taking the square root of the result.

RESULTS

Gravitational mass

The following graph shows the gravitational mass of NGC 1068 as a function of radius, calculated from its rotation curve. Error bars represent the uncertainties (Figure 9).

To visualize this in two dimensions, a circular colormap was used. The boundary of NGC 1068 was extracted from an image taken by the Hubble Space Telescope. The shape of the circular colormap was then adjusted to resemble the galaxy's image, and the two were overlaid for representation (Figure 10).

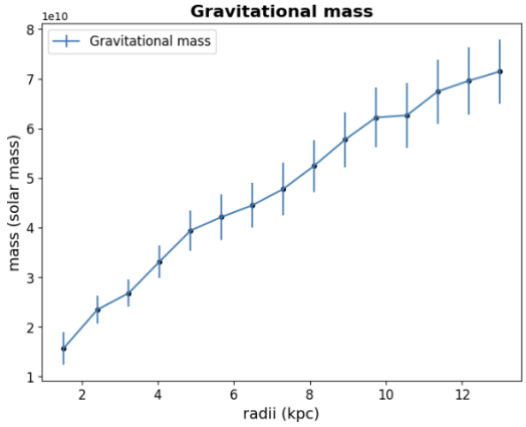

Figure 9. Gravitational mass distribution of NGC 1068.

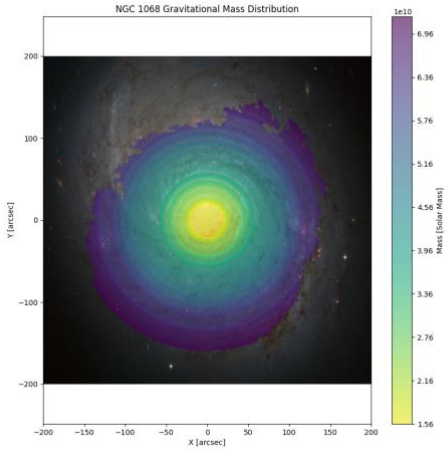

Figure 10. Colormap of the gravitational mass.

Photometry

From the results of linear regression for each filter, the values of *k* and ZP were obtained (Figure 11). Figure 12 shows the flux as a function of radius for each ugriz filter, presented in order from top to bottom as u, g, r, i, and z.

Comparing the observed flux in Jy units with data from the NASA Extragalactic Database (NED), it was found that the fluxes were smaller than those in NED: approximately 21% for the u-filter, 6% for the g-, r-, and i-filters, and 13% for the z-filter.

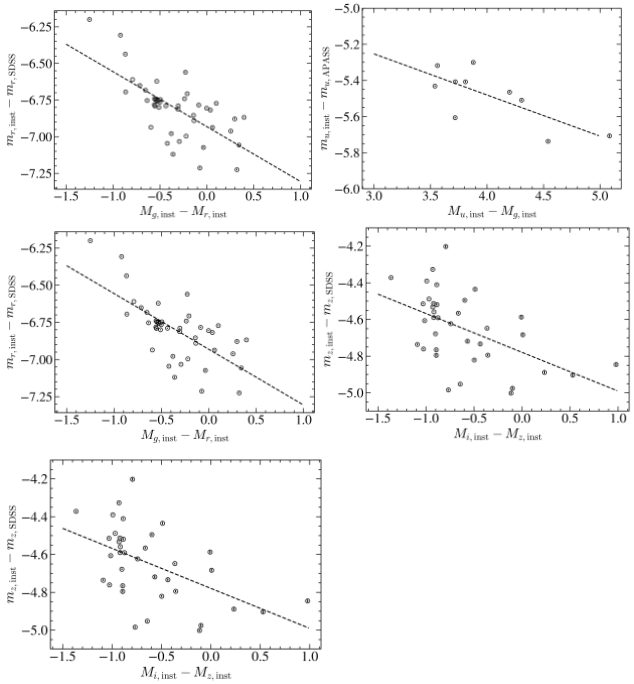

Figure 11. Linear regression results for the ugriz filters.

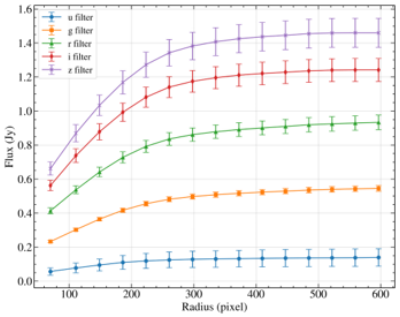

Figure 12. Flux as a function of radius for each ugriz filters (from top to bottom: u, g, r, i, z).

Stellar mass

The following results were obtained from running CIGALE, showing the best SED model for r = 1.5 kpc, the chi-squared distribution of stellar mass, the probability density function (PDF), and the radial distribution of stellar mass (Figures 13, 14, 15, 16, 17).

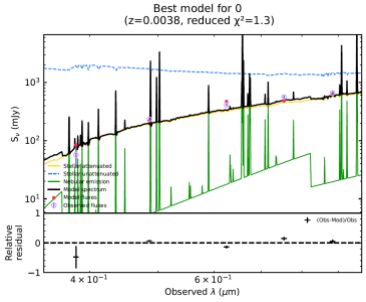

Figure 13. Best SED r = 1.5 kpc.

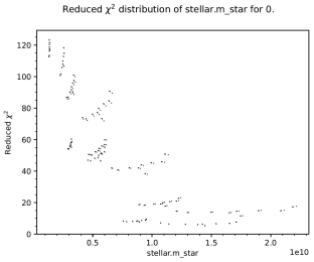

Figure 14. Chi-square distribution of stellar mass.

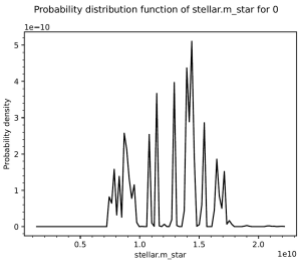

Figure 15: PDF of stellar mass r = 1.5 kpc.

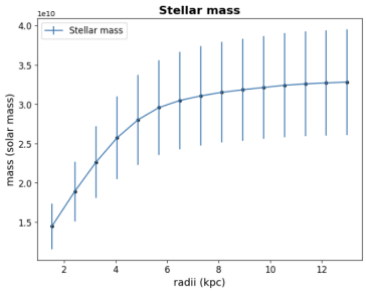

Figure 16. Stellar mass distribution of NGC 1068.

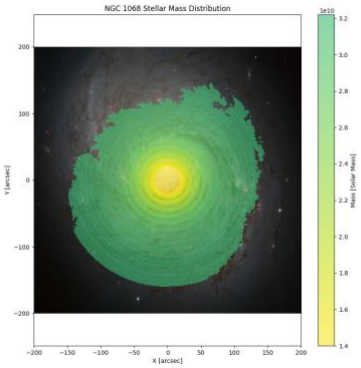

Figure 17. Colormap of the stellar mass distribution.

Dark Matter

The difference between gravitational and stellar mass increases with radius, and their 1σ error bars do not overlap beyond 1.5 kpc (Fig. 18), indicating a statistically significant discrepancy. This excess of gravitational mass relative to stellar mass is consistent with the presence of dark matter. The trend remains robust across the full radial range considered. This provides further evidence for the existence of dark matter, which interacts gravitationally but not electromagnetically, as revealed through dynamical analysis. Figures 19 and 20 present the resulting dark matter mass distribution of NGC 1068.

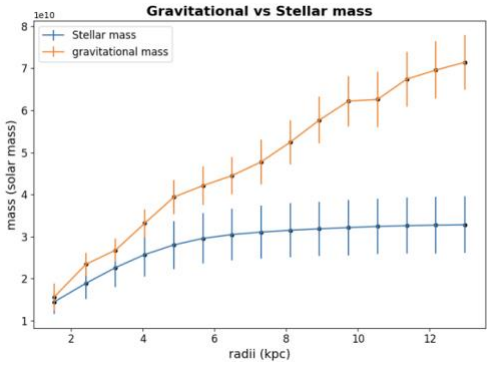

Figure 18. Gravitational mass vs Stellar mass in NGC 1068.

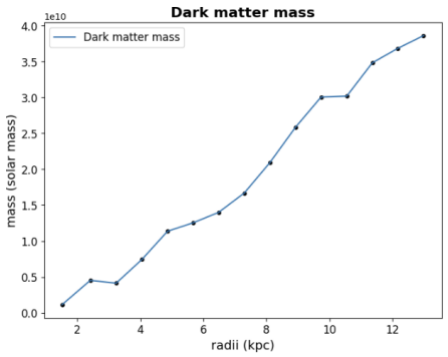

Figure 19. Dark matter mass distribution of NGC 1068.

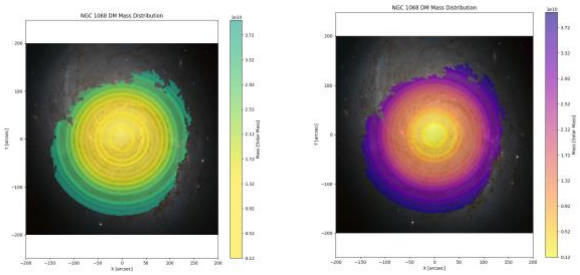

Figure 20. Dark matter colormap of NGC 1068.

DISCUSSION

Results of CIGALE

The residual map from the SED fitting shows that the error bars for the u-filter are abnormally large compared to other filters. This discrepancy likely stems from issues with the u-filter data or from fewer stars being detected during secondary calibration, compared to other filters. Given that the LSGT has a relatively small apertures of 0.43m, the accuracy of u-filter observations may have been low, even with longer exposure times.

Furthermore, the flux of galaxies and stars in the u-filter was observed to be smaller than in other filters. This could have introduced significant errors during the linear regression or background light subtraction processes.

Using a high-performance telescope would allow for more refined and accurate analyses. These enhancements could address the limitations identified above.

Dark matter mass estimation

Dark matter mass is typically calculated as the difference between the total dynamical mass of a galaxy and the combined mass of its stars and gas. However, in this study, gas mass was not included due to the lack of observational data in the radio and infrared wavelengths, where gas emissions are primarily detected. Estimating gas mass using optical data alone is unreliable and could lead to inaccurate results.[29,30] Additionally, the CIGALE modules for dust emission were omitted, further limiting the analysis. As a result, the dark matter mass estimation in this study considered only stellar mass, representing a key limitation.

The graph comparing gravitational mass and stellar mass indicates that the two are nearly identical in the central region, suggesting that dark matter is absent within approximately r = 1.5 kpc. This observation is another limitation of this study. NGC 1068 is a galaxy with strong AGN emissions at its center, but no AGN-related modules were configured in CIGALE. As a result, AGN emissions may have been misinterpreted as stellar emissions during the SED fitting process, leading to an overestimation of the stellar mass in the central region.[31,32] This issue is further exacerbated by the lack of infrared and AGN-related data, which led to the exclusion of relevant CIGALE modules—such as AGN, dust, and radio. Consequently, the stellar mass is likely overestimated in AGN-dominated regions, biasing the dark matter estimates within ~1.5 kpc. Since AGN emissions are predominantly observed in X-ray and radio wavelengths, which were not included in this study, likely contributing to the issue.

Securing observational data in the radio and X-ray wavelengths could address the limitations discussed above.

SED fitting in previous studies typically incorporates observational data across a broad wavelength range, using

measurements from approximately 10 to 20 filters. In contrast, this study relied on data from a narrow wavelength range and only five filters, which posed significant limitations. Consequently, the reliability of the dark matter mass distribution results is likely affected.

CONCLUSION

This study demonstrated the existence of dark matter and determined its distribution within a single galaxy, NGC 1068, using photometric data from the LSGT and its rotation curve.

Gravitational mass and its uncertainties were calculated from the rotation curve, and photometric data were generated to perform SED fitting with CIGALE. To ensure accurate photometric data, the study involved four key processes: identifying the galaxy's center, masking bright surrounding stars, conducting secondary calibration, and calculating photometric uncertainties through signal-to-noise ratio analysis and error propagation. From the SED fitting results, the optimal stellar mass and Bayesian errors were obtained. A comparison between the calculated stellar mass and gravitational mass confirmed the presence of dark matter, which cannot be observed through electromagnetic waves. Radial photometry was performed, and SED fitting results were obtained for each radius, allowing the determination of the dark matter distribution.

This study proposed a method for determining the dark matter mass distribution within a single galaxy, which can contribute to refining known dark matter density profiles (e.g. the NFW profile). Additionally, the results provide valuable insights into galaxy formation and evolution.

The significance of this study lies in its focus on a single galaxy. This offers a new direction for dark matter research, which has traditionally focused on larger-scale structures like galaxy clusters.

AUTHOR INFORMATION

Corresponding Author

Seonyu Lee – julius712@snu.ac.kr

Author Contributions

Seonyu Lee led the research from conception to execution, including designing the study, analyzing results, and writing the manuscript. Heeju Kim contributed to the photometric data analysis and data processing.

REFERENCES

[1] F. Zwicky, Die Rotverschiebung von extragalaktischen Nebeln. *Helv. Phys. Acta*. 6, 110-127 (1933). https://doi.org/10.5169/seals-110267

[2] V. C. Rubin, W. Ford, Jr. Kent, Rotation of the Andromeda Nebula from a spectroscopic survey of emission regions. *ApJ* 159, 379 (1970). https://doi.org/10.1086/150317

[3] M. Markevitch, *et al*., Direct constraints on the dark matter self-interaction cross. *ApJ* 606(2), 819-824 (2004). https://doi.org/10.1086/383178

[4] D. Clowe, *et al*., A direct empirical proof of the existence of dark matter. *ApJ* 648(2), L109-L113 (2006). https://doi.org/10.1086/508162

[5] M. A. Henson, D. J. Barnes, S. T. Kay, I. G. McCarthy, J. Schaye, The impact of baryons on massive galaxy clusters: halo structure and cluster mass estimates. *MNRAS*, 465(3), 3361-3378 (2017). https://doi.org/10.1093/mnras/stw2899

[6] K. G. Begeman, HI rotation curves of spiral galaxies. I. NGC 3198. *A&A* 223, 47-60 (1989).

[7] A. A. Dutton, A. V. Maccio, Cold dark matter haloes in the Planck era: evolution of structural parameters for Einasto and NFW profiles. *MNRAS* 441(4), 3359-3374 (2014). https://doi.org/10.1093/mnras/stu742

[8] V. Springel, et al., Simulations of the formation, evolution and clustering of galaxies and quasars. *Nature* 435(7042), 629-636 (2005). https://doi.org/10.1038/nature03597

[9] J. S. Bullock, M. Boylan-Kolchin, Small-scale challenges to the ΛCDM paradigm. *Annu. Rev. Astron. Astrophys*. 55, 343-387 (2017). https://doi.org/10.1146/annurev-astro-091916-055313

[10]E. Brinks, E. D. Skillman, R. J. Terlevich, E. Terlevich, HI Observations of NGC 1068. *Astrophys. Space. Sci.* 248, 23-31 (1997).

[11]G. Bruzual, S. Charlot, Stellar population synthesis at the resolution of 2003. *MNRAS* 344(4), 1000-1028 (2003). https://doi.org/10.1046/j.1365-8711.2003.06897.x

[12]D. Le Borgne, *et al*., Evolutionary synthesis of galaxies at high spectral resolution with the code PEGASE-HR. *A&A* 425, 881-897 (2004). https://doi.org/10.1051/0004-6361:200400044

[13]C. Conroy, Modeling the panchromatic spectral energy distributions of galaxies. *Annu. Rev. Astron. Astrophys*. 51, 393-455 (2013). https://doi.org/10.1146/annurev-astro-082812-141017

[14]C. Pacifici, *et al.*, The evolution of star formation histories of quiescent galaxies. *ApJ* 832(1), 79 (2016). https://doi.org/10.3847/0004-637X/832/1/79

[15]J. Walcher, B. Groves, T. Budavari, D. Dale, Fitting the integrated spectral energy distributions of galaxies. *Astrophys. Space. Sci.* 331(1), 1-51 (2011). https://doi.org/10.1007/s10509-010-0458-z

[16]J. J. Condon, Radio emission from normal galaxies. *Annu. Rev. Astron. Astrophys*. 30, 575-611 (1992). https://doi.org/10.1146/annurev.aa.30.090192.003043

[17]R. C. Kennicutt Jr., Star formation in galaxies along the Hubble sequence. *Annu. Rev. Astron. Astrophys.* 36, 189-232 (1998). https://doi.org/10.1146/annurev.astro.36.1.189

[18]K. Nandra, P. M. O'Neill, I. M. George, J. N. Reeves, An XMM-Newton survey of broad iron lines in Seyfert galaxies. *MNRAS* 382(1), 194-228 (2007). https://doi.org/10.1111/j.1365-2966.2007.12331.x

[19]S. Bianchi, E. M. Xilouris, The extent of dust in NGC 891 from Herschel/SPIRE images. *A&A* 531, L11 (2011). https://doi.org/10.1051/0004-6361/201116772

[20]M. Boquien, *et al*., CIGALE: a python Code Investigating GALaxy Emission. *A&A* 622, A103 (2019). https://doi.org/10.1051/0004-6361/201834156

[21]E. da Cunha, S. Charlot, D. Elbaz, A simple model to interpret the ultraviolet, optical and infrared emission from galaxies. *MNRAS* 388(4), 1595-1617 (2008). https://doi.org/10.1111/j.1365-2966.2008.13535.x

[22]C. Conroy, J. E. Gunn, M. White, The propagation of uncertainties in stellar population synthesis modeling. I. The relevance of uncertain aspects of stellar evolution and the initial mass function to the derived physical properties of galaxies. *ApJ* 699(1), 486-506 (2009). https://doi.org/10.1088/0004-637X/699/1/486

[23]K. Malek, *et al.*, HELP: modelling the spectral energy distributions of Herschel detected galaxies in the ELAIS N1 filed. *A&A* 620, A50 (2018). https://doi.org/10.1051/0004-6361/201833131

[24]A. K. Inoue, Rest-frame ultraviolet-to-optical spectral characteristics of extremely metal-poor and metal-free galaxies. *MNRAS* 415(3), 2920-2931 (2011). https://doi.org/10.1111/j.1365-2966.2011.18906.x

[25]S. Charlot, S. M. Fall, A simple model for the absorption of starlight by dust in galaxies. *ApJ* 539(2), 718-731 (2000). https://doi.org/10.1086/309250

[26]A. Meiksin, colour corrections for high-redshift objects due to intergalactic attenuation. *MNRAS* 365(3), 807-812 (2006). https://doi.org/10.1111/j.1365-2966.2005.09756.x

[27]B. M. Tinsley, Evolution of the stars and gas in galaxies. Fundam. Cosmic Phys. 5, 287-388 (1980). https://doi.org/10.48550/arXiv.2203.02041

[28]N. Gehrels, Confidence limits for small numbers of events in astrophysical data. *ApJ* 303, 336 (1986). https://doi.org/10.1086/164079

[29]J. R. Taylor, *An Introduction to Error Analysis: The Study of Uncertainties in Physical Measurements* (University Science Books, 1997).

[30]A. K. Leroy, *et al.*, The star formation efficiency in nearby galaxies: measuring where gas forms stars effectively. *Astron J* 136(6), 2782-2845 (2008). https://doi.org/10.1088/0004-6256/136/6/2782

[31]K. Iwasawa, A. C. Fabian, A. J. Young, H. Inoue, C. Matsumoto, Variation of the broad X-ray iron line in MCG-6-30-15 during a flare. *Mon. Not. R. Astron. Soc.* 306, L19-L24 (1999).

[32]M. Polleta, Spectral energy distributions of hard X-ray selected active galactic nuclei in the XMM-Newton medium deep survey. *ApJ* 663(1), 81-102 (2007). https://doi.org/10.1086/518113

COLUMBIA UNDERGRADUATE SCIENCE JOURNAL

Cardiac Regeneration: A Promising Future for Tissue Engineering and Cardiac Repair

Krishay Patel[1]

University of California, San Diego, La Jolla, CA, USA

KEYWORDS: Cardiac Regeneration, Cardiomyocytes, Cell Culture, Reprogramming, Tissue Engineering, Cardiovascular Disease, Imaging Techniques

ABSTRACT: Cardiovascular diseases are the leading cause of human death worldwide. These diseases have detrimental effects on the heart, damaging the tissue and disrupting healthy heart function. Cardiac functioning begins to dissipate as a result of cardiac cell death and subsequent damage to the structures of the heart. Cardiac regeneration is an evolving field in cardiac therapy that aims to rebuild damaged cardiac tissue that may have previously been beyond repair. Understanding how cardiac cells function within the heart is crucial in studying tissue engineering and cardiac regeneration. With the loss of cardiac cells following cardiovascular disease, the ability to extract healthy cardiac cells for tissue engineering becomes greatly limited. Thus, tissue cultures and cellular reprogramming become crucial methods for in vitro expansion of healthy cells. Understanding regeneration in the heart, cell sources necessary for cardiac regeneration, and the existing models that have been implemented for cardiac regeneration are crucial in advancing its study and improving methods to take cardiac regeneration to clinical trials. Imaging techniques to model patient-specific structures of the heart will ultimately help map damaged tissue, assisting with the entire regeneration process. Investigating the limitations of these techniques is equally important to improving cardiac regeneration, with the possibility to save countless lives.

INTRODUCTION

For many decades, cardiovascular-related diseases (CVDs) have been the leading cause of death globally as well as a major contributor to disabilities.[1] Despite advancements in medical care that have resulted in a decline in age-standardized CVD deaths occurring globally, the total CVD global deaths have continued to increase over the last three decades, and previous progress in counteracting the mortality effects of CVDs has become uneven and begun to stall.[2] The risk of exposure to CVDs has become increasing prevalent, with changes in the ecological and geological environment, modifications in lifestyle, and shifts in social policies contributing to CVD risk.[3] As a result, there has been great concern about heart repair and treatment.

CVDs have been understood to irreversibly damage cardiomyocytes, the cells in the heart responsible for the contractile functions of the heart. This leads to the formation of scar tissue, ultimately damaging the structure and function of the heart.[4] The adult human heart has limited regenerative capacity and so regenerative medicine therapies have shed new hopes in repairing or even replacing damaged hearts.[5,6] The advancements in the field of tissue engineering, particularly concerning cell reprograming, the development of functional biomaterials, and the fabrication of biomimetic cardiac tissue, have gained traction in providing possible

avenues for tissue regeneration applications within the heart. Biomaterial-based approaches have gained increasing attention for cardiac tissue engineering and regeneration after contributing to improved cardiac function, promoting angiogenesis, and diminishing severe immune responses following clinical trials on animals.[7]

Nevertheless, creating fully effective functional cardiac tissue in vitro is still a challenge in the field of tissue engineering, with the regeneration of an entire human organ in vitro, specifically the heart, being difficult in terms of specific chamber orientation and electrical function.[8] Despite this, implementations of tissue engineering to reconstruct cardiac tissue have reported better contractile function from the heart, and cardiac progenitor cells, responsible for contributing to cardiac tissue regeneration, have been reported to give rise to cardiomyocytes in vitro and in vivo after transplantation and to enhance cardiac function post-infarction.[9]

This review will highlight the progress made in the field of cardiac tissue engineering regarding regenerative tissue applications on the heart, with a particular focus on cell reprogramming in the context of tissue engineering, growing these cells in various culture media, and the applications of these cells within the cardiac tissue engineering process. An introduction to the cardiac system, along with the current status on regeneration and cell sources necessary to engineer cardiac tissue, and the experimental applications of working with the heart, including imaging techniques and the fabrication of biomimetic cardiac tissue, will also be discussed.

CARDIAC CELLS

Introduction to Cells

Cells are fundamental building blocks within an organism's body, present in all living organisms. They are responsible for carrying out all the vital functions, and they ultimately play a crucial role in organ function. In the process of regeneration, organisms have been shown to produce new cells when replacing an amputated, damaged structure.[10] Therefore, it remains crucial to produce and introduce new cells to the body when implementing regeneration after a particular body part or organ has faced severe damage. With cells being a crucial factor necessary for regeneration, it is crucial to produce the cells that predominantly make up the composition of the heart: cardiomyocytes.[11]

Cardiomyocytes are the striated, branched cardiac muscles found in the heart that are responsible for contracting together synchronously to enable the heart to work as a pump.[12] Following cardiac injury, a substantial number of cardiomyocytes are lost, and the heart forms a fibrotic scar to serve as patch where the cardiac muscle cells previously resided. However, the scar tissue does not maintain the ability to effectively contract.[13] In the event of a heart disease, one also observes cardiomyocyte cell death.[14] Therefore, combating the effects of CVDs and enhancing the possibilities of cardiac tissue regeneration can be made a possibility by exploring areas of cell reprogramming concerning cardiomyocytes, understanding how to culture these cells so that they can be reapplied within the human heart, and uncovering other cell sources necessary for cardiac tissue engineering.

Cell Culture

Cells occupy a crucial role in the functioning of organs, and damage to organs, such as CVDs, often results in the cells within that organ being damaged. As a result, the understanding and induction of cells to be introduced into the body becomes extremely important, particularly when discussing regeneration. However, to understand the cells within the body that are necessary for regenerative purposes and develop techniques to increase the number of required cells, these cells need to be extracted in vitro and grown outside the body. This is achieved through cell cultures.

Cell cultures are laboratory methods that enable the growth of eukaryotic or prokaryotic cells in physiological conditions. They enable the study of human health and diseases through the extraction of infected human cells, which can then be examined in a sterile, cultured environment. Utilizing the practice of cell cultures working with the homogeneity of clonal cell populations, specific cell types, and well-defined culture systems removes any interfering genetic or environmental confounding variables, thereby allowing data generation with high reproducibility, which may not otherwise be consistent when examining and working with an entire organ.[15] This then enables a possible avenue for inducing a high number of cardiomyocytes required for cardiac regeneration.

Among the various culture techniques available, two well-established models are 3D and 2D culture systems. 2D systems are the traditional monolayer cultures that are straightforward, cost-effective, and convenient for observation. However, 2D cultures fall short in simulating the in vivo morphology of the extra cellular matrix (ECM), and cells in these 2D cultures are compelled to adapt to their complex biological behaviors. These complications have resulted in a turn to 3D systems that better mimic the physiological context of the ECM.[16] 3D culture systems are more complex systems than 2D culture systems, as they have been developed to mimic in vivo conditions, and therefore provide a good alternative for the in vitro imitation of the human heart tissue. Generally divided into scaffold-based and scaffold-free, 3D heart tissue models allow cells to organize themselves into a 3D structure resembling the human myocardial cell organization. A major advantage of 3D cultures is that their more accurate imitation of the internal human environment allows researchers to better replicate in vitro cardiac tissue morphological, biochemical, and mechanical features.[17]

In the cardiovascular field, 3D culture systems are further differentiated into two categories; they either contain a scaffold matrix, generally a hydrogel, mixed with and populated by cells to form a strip shaped micro-tissue between attachment sites, or they are smaller cellular spheroids formed by self-assembly without scaffold proteins. An increasing number of studies have used a mix or co-culture several cell types, such as rodent and human induced pluripotent stem cell-derived cardiomyocytes.[18] In fact, larger tissue formats like multilayered cell sheets, re-cellularized hearts, or large biomaterial patches, which are too expensive and slow in manufacturing for drug testing, are developed for regenerative medicine, leading to advancements in issue and cardiac regeneration.[19]

Cell Reprogramming

Cellular reprogramming is the process by which cells can be reliably changed from one tissue type to another, enabling novel approaches to more deeply investigate the fundamental basis of cell identity.[20] The process of cellular reprogramming is not simply limited to a technique, but rather an application that can be used within the human body for regenerative purposes. The importance of maintaining high quantities of cardiomyocytes following CVDs remains a problem, and the issues extends to the fact that cardiomyocytes have little capability of proliferation after birth.[21] Through the process of trans differentiation, the conversion of one cell to another, cells that are abundant in the body can be reprogrammed into desired cell phenotypes to restore tissue function in damaged areas.[22] This process presents a possible avenue for further investigation into reprogramming the abundant cells in the body into the necessary cardiomyocytes, which may be scarce.

Several approaches for cellular reprogramming concerning the induction of cardiomyocytes have been investigated, and have proved successful in cardiomyocyte production, indicating a promising avenue towards cardiac tissue regeneration. Firstly, through combinatorial expression of two cardiac transcription factors, Gata4 and Tbx5, and a cardiac-specific subunit BAF chromatin-remodeling complex, Baf60c, the direct differentiation and conversion of mouse mesoderm into beating cardiomyocytes can occur.[23] Secondly, following experimentation using a combinatorial strategy, it was identified that a combination of microRNAs was capable of inducing direct cellular reprogramming of fibroblasts into cardiomyocyte-like cells in vitro.[24] Thirdly, by treating human fibroblasts with a combination of nine compounds, termed 9C, cardiomyocyte-like cells can be generated that uniformly contract and resemble human cardiomyocytes in their epigenetic properties.[25] Lastly, the introduction of three cardiogenic transcription factors: Gata4, Mef2c, and Tbx5 (GMT) can induce the direct reprogramming of cardiac fibroblasts into cardiomyocytes, and this discovery of the direct cardiac reprogramming factor GMT has also enabled the induction of cardiomyocytes inside the body.[26]

THE HEART AND ITS REGENERATIVE CAPABILITIES

Introducing the System of the Heart

The cardiovascular system is a crucial system within the body, composed of the heart, blood vessels, and blood. The cardiovascular system is designed to ensure the continuous survival of all cells within the body, which it achieves by maintaining the intermediate chemical environment of each cell in the body.[27] The heart remains at the center of the cardiovascular system, responsible for pumping blood through the pulmonary and systemic systems of the body. The cardiovascular system, in turn, serves as a body-wide network of vessels that transports nutrients, respiratory gases, metabolic waste, and hormones, distributes and dissipates heat, and assists in defending the body against disease.[28] The cardiovascular system, and ultimately the heart, plays a crucial role in the healthy function of the human body.

Adult hearts fail to regenerate following injury and CVDs, and this failure to regenerate myocardium is a crucial contributor to heart failure and ultimately death worldwide.[29]

Therefore, complications that occur within the cardiovascular system and affect the heart ultimately have a detrimental effect on the rest of the body, making the applications of regenerative medicine surrounding cardiac tissue more pressing.

Regeneration Within the Heart

Currently, experimentation in heart regeneration has been restricted to mouse model hearts. In a particular experiment, fetal rodent hearts that had undergone a specific genetic ablation were able to restore around 50% of the lost cardiomyocyte mass indicating that the embryonic environment and the transcriptional state of embryonic cardiomyocytes facilitate cardiomyocyte cell cycle re-entry and repopulation of the heart, an important discovery in understanding the regenerative potential from the embryo and the change thereafter following the first few weeks of life.[29] The field of heart regeneration has entered a period of extraordinary progress in the understanding of endogenous heart regeneration, stem cell differentiation for exogenous cell therapy, and cell-delivery methods.

However, the regenerative capacity expressed by adult individuals, human in particular, is not entirely favorable to generate cardiac tissue necessary following CVDs and injury. Although the heart retains the ability to regenerate in some lower vertebrates, adult mammals do not retain the capacity to replenish the heart with enough cardiomyocytes to restore function following injury. Therefore, the concept of heart and cardiac regeneration does not refer to a single area of study but rather encompasses the advancements and novel discoveries in fields including native cardiomyocyte renewal, cell therapy, direct reprogramming, and tissue engineering approaches to rebuild damaged heart tissue.[30]

Multiple approaches have been explored to promote and possibly achieve regeneration within the heart. Firstly, there are cell-free therapies for cardiac repair, where recombinant DNA, RNA-based, or protein therapeutics have been used in regenerative medicine. In myocardial infarction (MI) models, the injection of particular cardioactive growth factors, such as Neuregulin1, has induced sustained improvement in myocardial function.[31] Furthermore, the utilization of the cardiomyogenic factor Follistatin Like 1 can stimulate the recovery of contractile function and limit fibrosis following MI injury.[32] Secondly, cell-based therapies have been proposed as a promising approach for treating advanced heart failure and repairing damaged myocardial tissue. Thirdly, adult stem cell transplantations have been a possible avenue for cardiac regeneration. Experimental evidence suggests that adult stem cells, such as bone marrow cells, bone marrow purified hematopoietic stem cells, and bone marrow purified mesenchymal stem cells, can differentiate into cardiomyocytes. Lastly, pluripotent stem cell-based therapies have opened another path for cardiac regenerative possibilities. Specifically, it has been understood that human embryonic stem cells can differentiate into multiple cell types and thus have great therapeutic potential in regenerative medicine.[33]

Cell Sources

Cell sources for cardiac tissue engineering and regeneration refer to the variety of cell types that can be used in cardiac tissue engineering constructs. These cell types include cardiomyocytes, often derived from

induced pluripotent stem cells or isolated rodent hearts, cardiovascular cells, fibroblasts, various progenitor cells, stem cells, and spheroids.[34] Embryonic stem cells, as a type of stem cell, can be collected from the inner mass cells of blastocytes and can differentiate into cell types of all germ layers.[35] Through experimentation, cardio-intrusive cues were used to differentiate embryonic stem cells to cardiac progenitor cells and embed them in a fibrin patch, which in turn improved cardiac function. Induced pluripotent stem cells are widely used in regenerative medicine, and they are often obtained from a patient's somatic cells. These cells are similar to embryonic stem cells and have been used to regenerate the heart in a variety of animal studies. Cardiac stem cells, which can be acquired from the heart, are extremely useful for cardiac regenerative purposes, as they have the potential to self-renew and can differentiate into different cell types, such as vascular smooth muscle cells, cardiomyocytes, and endothelial cells.[36] Lastly, cardiac progenitor cells are defined by having self-renewing, clonogenic properties, as well as multipotent differentiation capabilities both in vivo and in vitro, which are desirable for promoting cardiac regeneration.[37]

At the core of the heart, however, lies cardiomyocyte-rich tissue to allow for rhythmic pump contractions. These cells appear to be the most prevalent cardiac cell population in the heart, and the need to acquire these cells is extremely important for regenerative applications to succeed.[6] Discovering sources to acquire cardiomyocyte cells is crucial to engineer cardiac tissue, and although there are existing limitations around human tissue availability, human adult cardiomyocytes can be isolated during myocardial biopsies.[38] However, this process needs to be done at quickly because following isolation, cardiomyocytes undergo a profound structural and functional remodeling, leading to cell differentiation and loss of viability.[39]

REGENERATIVE MODELS AND METHODS

Existing Models

There has been increasing demand for new therapeutic models, and such models are necessary to advance the understanding of the biological mechanisms of cardiac tissue regeneration, and test therapeutic approaches to regenerate tissue and restore cardiac function. In vitro model systems allow researchers to study biological systems while still maintaining a high level of control over the experimental parameters.[40] Such in vitro models include single cell models, 2D culture models, 3D culture models, coculture models, microfluidic system models, tissue models, whole heart models, and lastly cell sources as discussed in the previous section.

Examining the electromechanical properties of single cardiomyocytes has been crucial to the understanding of cardiac physiology. The electrophysiology of a single cardiomyocyte can be evaluated using the patch clamp technique, which can characterize the phenotype of CMs differentiated from embryonic stem cells.[41,42] Cardiomyocytes grown in 2D culture systems can elucidate molecular signaling pathways, assess the cardiotoxicity of a particular drug, and evaluate gene therapy approaches.[43,44,45] 3D models have been used as scaffolds to mimic the natural extracellular matrix, making the models extremely close to human myocardium, serving as models of healthy

human heart physiology.[40]

Cocultures systems enable a variety of growing cell types to be cultured together, which in turn stimulates the cellular communication that would normally occur between cells of different types.[46] The coculture of human embryonic stem cells with human umbilical-vein endothelial cells and mouse fibroblasts resulted in the formation of vascular networks resembling capillaries, and the coculture enhanced cardiomyocyte proliferation.[47] Microfluidic techniques make use of soft lithography techniques and have been constructed to study the electrophysiology of single cardiomyocytes in microfabricated patch-clamp devices or cell-to-cell signaling between pairs of cardiomyocytes.[48,49] These systems also make use of microfabrication techniques that provide advanced structure from well-defined scaffolds, which can improve drug discovery and better mimic heart physiology. Lastly, examining the whole heart of an organism outside its body allows for the evaluation of cardiac function ex vivo.

In vivo model systems provide a more accurate understanding of the complex behaviors of the heart within a living organism. In vivo model systems include noncardiac regenerative models and cardiac regenerative models. Noncardiac animal models, and noncardiac mammalian regeneration, can provided possible clues to cardiac regenerative biology using methods that are more practical because of lower cost and fewer technical and logistical challenges, and then can provide insight into potential mechanisms of cardiac regeneration. Cardiac regenerative models, on the other hand, focus on examining small and large animal mammalian models that have been studied extensively with the intention of discovering therapeutic interventions to effectively regenerate the heart and cardiac tissue following injury and CVDs.[40]

Advanced Optical Imaging Techniques

Optical imaging uses light and special properties of photons to obtain detailed images of organs, tissue, cells, and possibly even molecules.[50] Optical imaging is a non-invasive imaging technique that functions based on the absorption, scattering, and fluorescence properties of the incident particle. Optical imaging provides depth-resolved, high-resolution images of tissue microstructures in real time by measuring the interference between the light backscattered from the sample tissue and the light reflected from a reference. The use of optical imaging techniques can help understand a patient's heart structure, which can help prepare for procedures by identifying structures to avoid and locating areas for treatment and repair. The imaging plays a crucial role in early diagnosis of CVDs, as well as in monitoring and providing guidance for cardiac procedures. Due to the high resolution, fast imaging speeds, and non-invasive procedure obtained from optical imaging, this technique has seen increased clinical use over the past few decades.[51]

Molecular imaging, in particular optical imaging, has advanced in a way that allows for the characterization of biological processes at the cellular and subcellular levels, which could ultimately play a crucial role in the examination of cardiac tissue to understand their biological processes and whether tissue may be damaged or not.[52] Current methods of therapy for cardiac regeneration, including stem-cell therapy,

have been promising as discussed, but the challenges of such therapies are dependent on cell survival of the introduced cells, possible implantation difficulties due to adverse mechanical forces, and possible hypoxia However, the use of advanced optical imaging techniques has emerged as a novel approach to track engraftment, the formation of healthy blood cells following a transplant, as well as track the survival and rejection of transplanted tissue, which is crucial in understanding the efficacy of procedures conducted for cardiac regeneration, making this technique very valuable.[53,54]

Emerging Models to Constructure Cardiac Tissue

The majority of 3D cardiac models, until now, have been fabricated to be flat or small structures, which can limit volumetric expansion and functional maturation. The need to establish a model that could overcome these limitations of scale, maturity, and functionality of human cardiac tissues has been fabricated by integrating native heart-like cellular and extracellular components and dynamic flow. This new 3D human cardiac tissue model was successfully validated for various biomedical applications, including cardiotoxicity prediction, cardiac disease modeling, and regenerative therapy.[55] Together, this 3D tissue model is extremely beneficial in imaging the heart and its cardiac tissue with respect to identity and predicting the presence of cardiac disease, as well as applying this model for cardiac regeneration.

With the current shortage of heart donors available and the urgent need for new sources of cardiac regeneration medicine, tissue engineering using bioactive materials and 3D bioprinting to create microscale cardiac tissue has shown great advantages and promise in the field of cardiac regenerative therapy. 3D bioprinting focuses on the tight fitting of a sufficient number of functional cardiomyocytes with a feasible scaffold on a small scale.[56]

3D bioprinting has ultimately emerged as an approach for in vitro generation of functional cardiac tissue for drug screening and cardiac regenerative therapy. The use of 3D bioprinted cardiac patches, fabricated by human coronary artery endothelial cells, collagen microprinting, and an alginate matrix, resulted in high levels of cell proliferation and differentiation, which are crucial for regeneration of cardiac tissue. 3D bioprinting is a layer-by-layer additive technology that precisely deposits biomaterials and active cells in accordance with a certain spatial pattern that has high resolution simulation of the heart.[57]

Using a combination of different bioprinting approaches, a variety of cardiac constructs, including cartilage and a heart valve, have been successfully constructed, which is crucial to repair damaged tissue structures within the heart. Experiments show that bioprinted cardiac tissue possess cardiomyocytes orientated in an organized fashion and contracting capabilities, both consist with native heart tissue characteristics.[57,58]

Fabrication of Biomimetic Cardiac Tissues

Inducing the maturation of cardiomyocytes remains a problem in the field of cardiac tissue engineering and cardiac regeneration. Specifically, addressing this issue within the complexity of the in vivo conditions of the human heart remains an important barrier in cardiac tissue engineering. A variety of

methods have been tested to grow biomimetic tissue in the laboratory that can adjust to the

complexities within the body. These methods include the Hydrogel method, decellularized bio scaffolds, microfabrication, and bioprinting as discussed in the previous section. Hydrogels are widely used for their ability to be molded into several geometries and their scalability. The cardiac tissue can be fabricated by joint gelatin of cells and a polymer or by having a casting mold to confine the cells in a particular organization, which can mimic cell organization found in native cardiac tissue by freeze-drying the hydrogel.[6]

Decellularized bio scaffolds aim to generate scaffolds with a native extracellular matrix ultrastructure and composition while removing all cells and genetic material present in the native tissue. The most immediate application of decellularized myocardial sheets is scaffold recellularization; however, the recellularization of such sheets with cardiomyocytes, which can be successfully achieved, does not translate to the goal of recellularizing human hearts, which requires a vast number of cardiomyocytes for which there is no current sustainable production method.[6]

The use of biomaterials with built-in electroconductive characteristics are used to mimic the electrical conductivity of the native heart tissue, and scaffolds infused with electroconductive elements create a conductive network across the constructed tissue, which imitate electrical conductivity seen in the heart.[59] Gelatin-based scaffolds have also gained attention in recent years with their great bio-affinity that encourages the regeneration of tissue, and how by strengthening such gelatin-based scaffolds, the natural tissue can be accurately mimicked. Gelatin-based scaffolds cansimplify the inclusion of cells and growth factors for optimal scaffold construction, and advanced production strategies for these scaffolds create highly configurable scaffold geometric shapes needed for specific medical necessities and to fabricate patient-specific implants.[60]

Advances in microfabrication have allowed for the detailed engineering of material features to resemble the in vivo conditions of an organ, particularly the heart. Simpler systems use microfabrication to pattern material substrates, to ease cardiomyocyte spreading and sarcomere axial alignment, and following experimentation, a substantial improvement in cardiomyocyte alignment was shown. Microfabrication methodologies can ultimately be harnessed to create complex tissues like the native myocardium, which is crucial for regenerative cardiac tissue to adjust to the in vivo construct and conditions of the native cardiac tissue.[6]

Limitations of Imaging Methods for the Heart

The rapid and complex changes that occur from heart morphology make imaging the heart during development a challenging task. Confocal microscopy, an advancement of fluorescence microscopy, offers higher spatial resolution and the ability to visualize subcellular details; however, this imaging technique is relatively slow and harsh on the sample, potentially causing phototoxicity and bleaching.[61,62] A major challenge in biomimetic cardiac tissue engineering is the scalability of the fabrication technique and the translation of these approaches to clinical

applications. The issues that remain around biomimetic cardiac tissue engineering include standardized production methods, optimizing functional and structural maturation, and ensuring long-term stability of synthetic cardiac tissue.[59] These challenges, ultimately, require significant attention to move forward with advancements in this field.

The advancements in 3D bioprinting have revolutionized potential avenues in cardiac treatment in the future, with the opportunity to fabricate microscale cardiac tissue for potential in vivo applications. However, limitations occur with the use of artificial prints, compared to the original hearts of large mammals, as these prints remain naïve in their generation of both the input and output mechanical strengths long-term. Furthermore, because of the complexity of heart movement, whether these 3D bioengineered bodies are able to achieve or even get close to perfect cardiac replication physically and chemically remains unknown.[56]

There are a vast number of imaging techniques to examine the cardiac system, and although there are specific advantages for each imaging technique that make these applicable in certain situations, each of them has their own limitations. These imaging techniques include radionuclide imaging, MRI, ultrasound, CT scan, optical imaging, and magnetic particle imaging (MPI).

Radionuclide imaging has the limitations of radioactive exposure, high cost of operation, poor spatial resolution, and a short imaging time. MRIs are also expensive and require heavy involvement to operate. Ultrasounds have low tissue contrast, and they are dependent on an operator. CT scans have ionizing radiation which is extremely dangerous, and they offer limited soft tissue discrimination. Optical imaging offers poor penetration depth, poor spatial resolution, and it is only used in preclinical trials. Lastly, MPIs are unable to discriminate live cells from dead cells.

CONCLUSION

CVDs have had a fatal impact on the human population. Thus, studying heart and cardiac tissue repair has become a forefront issue to combat the effects of CVDs. The effects of CVDs result in damage of cardiac tissue and the death of cardiac cells. The heart soon experiences degraded function, triggering other dysfunctions within the body that ultimately result in death. Therefore, exploring human regenerative capacity and the potential application of heart and cardiac regeneration has evolved as a new therapeutic to engineering functional cardiac tissue following CVDs. The potential of cardiac regeneration is very promising for cardiac repair, and the progress made in the field through tissue engineering has shown the beneficial outcomes that can be achieved through cardiac regeneration.

The focus on the production of cardiac cells following CVDs is crucial in restoring appropriate cardiac function. Cells form the basis of living tissue, making the induction of cells important for regenerative purposes, especially cardiomyocytes which once introduced into the body are important for cardiac function. Through various applications of cell culture, specifically 2D and 3D cultures, these cardiac cells can be effectively understood and examined. Growing these cells in an artificial environment is extremely important in the context of cardiac

regeneration, as more cardiac cells can be produced and introduced into the human body as a supplement to compensate for the loss of cells following cell death. Cellular reprogramming also plays a crucial role in cardiac regeneration, by allowing cells to be changed to another cell type which could assist the process of cardiac regeneration by differentiating greater populated cells into cardiomyocytes which are less abundant in the body.

The field of cardiac regeneration actively growing, with a variety of approaches being explored to help promote and achieve regeneration of the heart. Cells sources have also been of extreme importance in engineering cardiac tissue to contribute towards regeneration of the heart. Cells sources for cardiac tissue engineering refer to the variety of cell types that can be used in cardiac tissue engineering constructs, including cardiomyocytes, induced pluripotent stem cells or isolated rodent hearts, cardia vascular cells and fibroblasts, various progenitor and stem cells and spheroids. Discovering and utilizing various cells sources to acquire cardiomyocyte cells is crucial to engineer cardiac tissue, as these cells appear to be the most prevalent cardiac cell population in the heart, and the need to acquire these cells is extremely important for regenerative applications to succeed.[6]

Various existing models have helped propel the concept of cardiac regeneration to become a forefront technique for therapeutics in the future to treat damaged cardiac tissue. The use of a variety of imaging techniques has been crucial in allowing internal areas of the cardiac system and the heart, as well as problems with a particular person's heart, to be examined and understood externally. This is crucial in cardiac regeneration, in particular, as particular constructs of cardiac tissue could then be induced after understanding a person's current heart state and the areas that are damaged. The utilization of imaging techniques also showcases the efficacy of the regenerative tissue and its ability to work within the body, which is useful when evaluating the use of the construct and understanding how it contribute to regeneration through a non-invasive procedure. However, the use of imaging techniques, and the development of models relating to cardiac regeneration have their inherent limitations, serving as a setback for the progress of cardiac regeneration. The need to address these issues is crucial in developing therapeutics and constructs that can advance cardiac regeneration and better suit their applications for human use. Possible directions for future myocardial regeneration include the consolidation of transplantation of cells with "true" regenerative potential, tissue engineering with various scaffolds and cell types, a stimulation of resident cell sources by cytokines or growth factors, and a direct reprogramming of scar tissue by delivery of various transcription factors or miRNAs63.

Cardiac regeneration is shaping to be a promising field in the future to treat damaged cardiac tissue following CVDs. The applications of cardiac regeneration are endless, and the hope generated by the possibility of cardiac regeneration is likely to be carried into the future. The process of cardiac regeneration could ultimately

revolutionize cardiac tissue repair and treatment, and the promise of cardiac regeneration could be the step needed to save countless lives.

AUTHOR INFORMATION

Corresponding Author

Krishay Patel – krishay.in.sa@gmail.com

Author Contributions

Krishay Patel provided full contribution to the research and writing of the manuscript. The manuscript was drafted through the Collegiate Mentorship Program with the help of Dr Rosalyn Abbott (rabbott@andrew.cmu.edu)

REFERENCES

[1] Kauffman, D. (n.d.). Cardiovascular Disease Burden, Deaths Are Rising Around the World. American College of Cardiology. https://www.acc.org/about-acc/press-releases/2020/12/09/18/30/http%3a%2f%2fwww.acc.org%2fabout-acc%2fpress-releases%2f2020%2f12%2f09%2f18%2f30%2fcvd-burden-and-deaths-rising-around-the-world

[2] Di Cesare, M., Bixby, H., Gaziano, T., Hadeed, L., Kabudula, C., Vaca McGhie, D., Mwangi, J., Pervan, B., Perel, P., Piñeiro, D., Taylor, S., & Pinto, F. (n.d.). World Heart Report 2023 Confronting The Worlds Number One Killer. World Heart Federation. https://world-heart-federation.org/wp-content/uploads/World-Heart-Report-2023.pdf

[3] Bhatnagar, A. (2017). Environmental Determinants of Cardiovascular Disease. Circulation Research, 121(2), 162–180. https://doi.org/10.1161/CIRCRESAHA.117.306458

[4] Hotkar, A. J., & Balinsky, W. (2012). Stem cells in the treatment of cardiovascular disease—An overview. Stem Cell Reviews and Reports, 8(2), 494–502. https://doi.org/10.1007/s12015-011-9302-2

[5] Bergmann, O. et al. Evidence for cardiomyocyte renewal in humans. Science 324, 98–102 (2009).

[6] Tenreiro, M. F., Louro, A. F., Alves, P. M., & Serra, M. (2021). Next generation of heart regenerative therapies: Progress and promise of cardiac tissue engineering. Npj Regenerative Medicine, 6(1), 1–17. https://doi.org/10.1038/s41536-021-00140-4

[7] Scafa Udriște, A., Niculescu, A.-G., Iliuță, L., Bajeu, T., Georgescu, A., Grumezescu, A. M., & Bădilă, E. (2023). Progress in Biomaterials for Cardiac Tissue Engineering and Regeneration. Polymers, 15(5), 1177. https://doi.org/10.3390/polym15051177

[8] Zhao, Y., Rafatian, N., Wang, E. Y., Wu, Q., Lai, B. F. L., Lu, R. X., Savoji, H., & Radisic, M. (2020). Towards chamber specific heart-on-a-chip for drug testing applications. Advanced Drug Delivery Reviews, 165–166, 60. https://doi.org/10.1016/j.addr.2019.12.002

[9] Laflamme, M. A., & Murry, C. E. (2011). Heart Regeneration. Nature, 473(7347), 326–335. https://doi.org/10.1038/nature10147

[10] King, R. S., & Newmark, P. A. (2012). The cell biology of regeneration. The Journal of Cell Biology, 196(5), 553–562. https://doi.org/10.1083/jcb.201105099

[11] Arackal, A., & Alsayouri, K. (2024). Histology, Heart. In StatPearls. StatPearls Publishing. http://www.ncbi.nlm.nih.gov/books/NBK545143/

[12] Ripa, R., George, T., Shumway, K. R., & Sattar, Y. (2024). Physiology, Cardiac Muscle. In StatPearls. StatPearls Publishing. http://www.ncbi.nlm.nih.gov/books/NBK572070/

[13] Patel, P., & Karch, J. (2020). Chapter Four—Regulation of cell death in the cardiovascular system. In J. K. E. Spetz & L. Galluzzi (Eds.), International Review of Cell and Molecular Biology (Vol. 353, pp. 153–209). Academic Press. https://doi.org/10.1016/bs.ircmb.2019.11.005

[14] Chiong, M., Wang, Z. V., Pedrozo, Z., Cao, D. J., Troncoso, R., Ibacache, M., Criollo, A., Nemchenko, A., Hill, J. A., & Lavandero, S. (2011). Cardiomyocyte death: Mechanisms and translational implications. Cell Death & Disease, 2(12), e244. https://doi.org/10.1038/cddis.2011.130

[15] Segeritz, C.-P., & Vallier, L. (2017). Cell Culture. Basic Science Methods for Clinical Researchers, 151–172. https://doi.org/10.1016/B978-0-12-803077-6.00009-6

[16] Sun, S., Liu, Y., Gao, H., Guan, W., Zhao, Y., & Li, G. (2024). Cell culture on suspended fiber for tissue regeneration: A review. International Journal of Biological Macromolecules, 268, 131827. https://doi.org/10.1016/j.ijbiomac.2024.131827

[17] Gisone, I., Cecchettini, A., Ceccherini, E., Persiani, E., Morales, M. A., & Vozzi, F. (2022). Cardiac tissue engineering: Multiple approaches and potential applications. Frontiers in Bioengineering and Biotechnology, 10, 980393. https://doi.org/10.3389/fbioe.2022.980393

[18] Zuppinger, C. (2019). 3D Cardiac Cell Culture: A Critical Review of Current Technologies and Applications. Frontiers in Cardiovascular Medicine, 6, 87. https://doi.org/10.3389/fcvm.2019.00087

[19] Jackman, C. P., Ganapathi, A. M., Asfour, H., Qian, Y., Allen, B. W., Li, Y., & Bursac, N. (2018). Engineered cardiac tissue patch maintains structural and electrical properties after epicardial implantation. Biomaterials, 159, 48–58. https://doi.org/10.1016/j.biomaterials.2018.01.002

[20] Wilmut, I., Sullivan, G., & Chambers, I. (2011). The evolving biology of cell reprogramming. Philosophical Transactions of the Royal Society B: Biological Sciences, 366(1575), 2183–2197. https://doi.org/10.1098/rstb.2011.0051

[21] Kuang, J., Huang, T., & Pei, D. (2022). The Art of Reprogramming for Regenerative Medicine. Frontiers in Cell and Developmental Biology, 10, 927555. https://doi.org/10.3389/fcell.2022.927555

[22] Grath, A., & Dai, G. (2019). Direct cell reprogramming for tissue engineering and regenerative medicine. Journal of Biological Engineering, 13(1), 14. https://doi.org/10.1186/s13036-019-0144-9

[23] Takeuchi, J. K., & Bruneau, B. G. (2009). Directed transdifferentiation of mouse mesoderm to heart tissue by defined factors. Nature, 459(7247), 708–711. https://doi.org/10.1038/nature08039

[24] Jayawardena, T. M., Egemnazarov, B., Finch, E. A., Zhang, L., Payne, J. A., Pandya, K., Zhang, Z., Rosenberg, P., Mirotsou, M., & Dzau, V. J. (2012). MicroRNA-mediated in vitro and in vivo Direct Reprogramming of Cardiac Fibroblasts to Cardiomyocytes. Circulation Research, 110(11), 1465–1473. https://doi.org/10.1161/CIRCRESAHA.112.269035

[25] Cao, N., Huang, Y., Zheng, J., Spencer, C. I., Zhang, Y., Fu, J.-D., Nie, B., Xie, M., Zhang, M., Wang, H., Ma, T., Xu, T., Shi, G., Srivastava, D., & Ding, S. (2016). Conversion of human fibroblasts into functional cardiomyocytes by small molecules. Science (New York, N.Y.), 352(6290), 1216–1220. https://doi.org/10.1126/science.aaf1502

[26] Yamakawa, H., & Ieda, M. (2021). Cardiac regeneration by direct reprogramming in this decade and beyond. Inflammation and Regeneration, 41, 20. https://doi.org/10.1186/s41232-021-00168-5

[27] Pittman, R. N. (2011). The Circulatory System and Oxygen Transport. In Regulation of Tissue Oxygenation. Morgan & Claypool Life Sciences. https://www.ncbi.nlm.nih.gov/books/NBK54112/

[28] Stephenson, A., Adams, J. W., & Vaccarezza, M. (2017). The vertebrate heart: An evolutionary perspective. Journal of Anatomy, 231(6), 787–797. https://doi.org/10.1111/joa.12687

[29] Uygur, A., & Lee, R. T. (2016). Mechanisms of Cardiac Regeneration. Developmental Cell, 36(4), 362–374. https://doi.org/10.1016/j.devcel.2016.01.018

[30] Garbern, J. C., & Lee, R. T. (2022). Heart regeneration: 20 years of progress and renewed optimism. Developmental Cell, 57(4), 424–439. https://doi.org/10.1016/j.devcel.2022.01.012

[31] Bersell, K., Arab, S., Haring, B., & Kühn, B. (2009). Neuregulin1/ErbB4 signaling induces cardiomyocyte proliferation and repair of heart injury. Cell, 138(2), 257–270. https://doi.org/10.1016/j.cell.2009.04.060

[32] Wei, K., Serpooshan, V., Hurtado, C., Diez-Cuñado, M., Zhao, M., Maruyama, S., Zhu, W., Fajardo, G., Noseda, M., Nakamura, K., Tian, X., Liu, Q., Wang, A., Matsuura, Y., Bushway, P., Cai, W., Savchenko, A., Mahmoudi, M., Schneider, M. D., … Ruiz-Lozano, P. (2015). Epicardial FSTL1 reconstitution regenerates the adult mammalian heart. Nature, 525(7570), 479–485. https://doi.org/10.1038/nature15372

[33] Wang, J., An, M., Haubner, B. J., & Penninger, J. M. (2023). Cardiac regeneration: Options for repairing the injured heart. Frontiers in Cardiovascular Medicine, 9, 981982. https://doi.org/10.3389/fcvm.2022.981982

[34] Cell sources for cardiac tissue engineering. A variety of cell types... (n.d.). ResearchGate https://www.researchgate.net/figure/Cell-sources-for-cardiac-tissue-engineering-A-variety-of-cell-types-can-be-used-in_fig2_349634500

[35] Müller, P., Lemcke, H., & David, R. (2018). Stem Cell Therapy in Heart Diseases—Cell Types, Mechanisms and Improvement Strategies. Cellular Physiology and Biochemistry: International Journal of Experimental Cellular Physiology, Biochemistry, and Pharmacology, 48(6), 2607–2655. https://doi.org/10.1159/000492704

[36] Boroumand, S., Haeri, A., Nazeri, N., & Rabbani, S. (2021). Review Insights In Cardiac Tissue Engineering: Cells, Scaffolds, and Pharmacological Agents. Iranian Journal of Pharmaceutical Research : IJPR, 20(4), 467–496. https://doi.org/10.22037/IJPR.2021.114730.150124

[37] Mauretti, A., Spaans, S., Bax, N. A. M., Sahlgren, C., & Bouten, C. V. C. (2017). Cardiac Progenitor Cells and the Interplay with Their Microenvironment. Stem Cells International, 2017, 7471582. https://doi.org/10.1155/2017/7471582

[38] Watson, S. A., Scigliano, M., Bardi, I., Ascione, R., Terracciano, C. M., & Perbellini, F. (2017). Preparation of viable adult ventricular myocardial slices from large and small mammals. Nature Protocols, 12(12), 2623–2639. https://doi.org/10.1038/nprot.2017.139

[39] Banyasz, T., Lozinskiy, I., Payne, C. E., Edelmann, S., Norton, B., Chen, B., Chen-Izu, Y., Izu, L. T., & Balke, C. W. (2008). Transformation of adult rat cardiac myocytes in primary culture. Experimental Physiology, 93(3), 370–382. https://doi.org/10.1113/expphysiol.2007.040659

[40] Garbern, J. C., Mummery, C. L., & Lee, R. T. (2013). Model Systems for Cardiovascular Regenerative Biology. Cold Spring Harbor Perspectives in Medicine, 3(4), a014019. https://doi.org/10.1101/cshperspect.a014019

[41] Cerbai, E., Sartiani, L., De paoli, P., & Mugelli, A. (2000). ISOLATED CARDIAC CELLS FOR ELECTROPHARMACOLOGICAL STUDIES. Pharmacological Research, 42(1), 1–8. https://doi.org/10.1006/phrs.1999.0654

[42] Maltsev, V. A., Wobus, A. M., Rohwedel, J., Bader, M., & Hescheler, J. (1994). Cardiomyocytes differentiated in vitro from embryonic stem cells developmentally express cardiac-specific genes and ionic currents. Circulation Research, 75(2), 233–244. https://doi.org/10.1161/01.res.75.2.233

[43] von Gise, A., Lin, Z., Schlegelmilch, K., Honor, L. B., Pan, G. M., Buck, J. N., Ma, Q., Ishiwata, T., Zhou, B., Camargo, F. D., & Pu, W. T. (2012). YAP1, the nuclear target of Hippo signaling, stimulates heart growth through cardiomyocyte proliferation but not hypertrophy. Proceedings of the National Academy of Sciences of the United States of America, 109(7), 2394–2399. https://doi.org/10.1073/pnas.1116136109

[44] Estimating the risk of drug-induced proarrhythmia using human induced pluripotent stem cell-derived cardiomyocytes—PubMed. (n.d.). https://pubmed.ncbi.nlm.nih.gov/21693436/

[45] Improving cardiac conduction with a skeletal muscle sodium channel by gene and cell therapy—PMC. (n.d.). https://www.ncbi.nlm.nih.gov/pmc/articles/PMC3392452/

[46] Kirkpatrick, C. J., Fuchs, S., & Unger, R. E. (2011). Co-culture systems for vascularization—Learning from nature. Advanced Drug Delivery Reviews, 63(4–5), 291–299. https://doi.org/10.1016/j.addr.2011.01.009

[47] Stevens, K. R., Kreutziger, K. L., Dupras, S. K., Korte, F. S., Regnier, M., Muskheli, V., Nourse, M. B., Bendixen, K., Reinecke, H., & Murry, C. E. (2009). Physiological function and transplantation of scaffold-free and vascularized human cardiac muscle tissue. Proceedings of the National Academy of Sciences of the United States of America, 106(39), 16568–16573. https://doi.org/10.1073/pnas.0908381106

[48] Mammalian electrophysiology on a microfluidic platform—PMC. (n.d.). https://www.ncbi.nlm.nih.gov/pmc/articles/PMC1166618/

[49] Klauke, N., Smith, G., & Cooper, J. M. (2007). Microfluidic systems to examine intercellular coupling of pairs of cardiac myocytes. Lab on a Chip, 7(6), 731–739. https://doi.org/10.1039/b706175g

[50] Optical Imaging. (n.d.). National Institute of Biomedical Imaging and Bioengineering. https://www.nibib.nih.gov/science-education/science-topics/optical-imaging

[51] Hendon, C. P., Lye, T. H., Yao, X., Gan, Y., & Marboe, C. C. (2019). Optical coherence tomography imaging of cardiac substrates. Quantitative Imaging in Medicine and Surgery, 9(5), 882–904. https://doi.org/10.21037/qims.2019.05.09

[52] Janib, S. M., Moses, A. S., & MacKay, J. A. (2010). Imaging and drug delivery using theranostic nanoparticles. Advanced Drug Delivery Reviews, 62(11), 1052–1063. https://doi.org/10.1016/j.addr.2010.08.004

[53] Roura, S., Gálvez-Montón, C., & Bayes-Genis, A. (2013). Bioluminescence imaging: A shining future for cardiac regeneration. Journal of Cellular and Molecular Medicine, 17(6), 693–703. https://doi.org/10.1111/jcmm.12018

[54] Cao, Y.-A., Bachmann, M. H., Beilhack, A., Yang, Y., Tanaka, M., Swijnenburg, R.-J., Reeves, R., Taylor-Edwards, C., Schulz, S., Doyle, T. C., Fathman, C. G., Robbins, R. C., Herzenberg, L. A., Negrin, R. S., & Contag, C. H. (2005). Molecular imaging using labeled donor tissues reveals patterns of engraftment, rejection, and survival in transplantation. Transplantation, 80(1), 134–139. https://doi.org/10.1097/01.tp.0000164347.50559.a3

[55] Min, S., Kim, S., Sim, W.-S., Choi, Y. S., Joo, H., Park, J.-H., Lee, S.-J., Kim, H., Lee, M. J., Jeong, I., Cui, B., Jo, S.-H., Kim, J.-J., Hong, S. B., Choi, Y.-J., Ban, K., Kim, Y.-G., Park, J.-U., Lee, H.-A., … Cho, S.-W. (2024). Versatile human cardiac tissues engineered with perfusable heart extracellular microenvironment for biomedical applications. Nature Communications, 15(1), 2564. https://doi.org/10.1038/s41467-024-46928-y

[56] Liu, N., Ye, X., Yao, B., Zhao, M., Wu, P., Liu, G., Zhuang, D., Jiang, H., Chen, X., He, Y., Huang, S., & Zhu, P. (2020). Advances in 3D bioprinting technology for cardiac tissue engineering and regeneration. Bioactive Materials, 6(5), 1388–1401. https://doi.org/10.1016/j.bioactmat.2020.10.021

[57] Frontiers | 3D Bioprinting Technology – One Step Closer Towards Cardiac Tissue Regeneration. (n.d.). https://www.frontiersin.org/articles/10.3389/fmats.2021.804134/full

[58] Kato, B., Wisser, G., Agrawal, D. K., Wood, T., & Thankam, F. G. (2021). 3D bioprinting of cardiac tissue: Current challenges and perspectives. Journal of Materials Science. Materials in Medicine, 32(5). https://doi.org/10.1007/s10856-021-06520-y

[59] Biomimetic Approaches in Cardiac Tissue Engineering: Replicating the Native Heart Microenvironment—PMC. (n.d.). https://www.ncbi.nlm.nih.gov/pmc/articles/PMC10423641/

[60] Rashid, A. B., Showva, N.-N., & Hoque, M. E. (2023). Gelatin-based scaffolds: An intuitive support structure for regenerative therapy. Current Opinion in Biomedical Engineering, 26, 100452. https://doi.org/10.1016/j.cobme.2023.100452

[61] Raiola, M., Sendra, M., & Torres, M. (2023). Imaging Approaches and the Quantitative Analysis of Heart Development. Journal of Cardiovascular Development and Disease, 10(4), 145. https://doi.org/10.3390/jcdd10040145

[62] Fluorescence Microscopy—An Outline of Hardware, Biological Handling, and Fluorophore Considerations—PMC. (n.d.). https://www.ncbi.nlm.nih.gov/pmc/articles/PMC8750338/

[63] Doppler, S. A., Deutsch, M.-A., Lange, R., & Krane, M. (2013). Cardiac regeneration: Current therapies—future concepts. Journal of Thoracic Disease, 5(5). https://doi.org/10.3978/j.issn.2072-1439.2013.08.71